Hirsch, K. K., Bauer, K., Scheck-Wenderoth, M. (2009): Deep structure of the western South African passive margin - Results of a combined approach of seismic, gravity and isostatic investigations. - Tectonophysics, 470, 1-2, 57-70

DOI: 10.1016/j.tecto.2008.04.028

Deep structure of the western South African passive margin - results of a combined approach of seismic, gravity and isostatic investigations

Katja K. Hirsch[1], Klaus Bauer[2], Magdalena Scheck-Wenderoth[3]

[1]GeoForschungsZentrum Potsdam, Telegrafenberg, 14473 Potsdam, Germany: hirsch@gfz-potsdam.de, Fax: +49 -331-288-1349 (corresponding author)

[2]GeoForschungsZentrum Potsdam, Telegrafenberg, 14473 Potsdam, Germany: klaus@gfz-potsdam.de, Fax: +49 -331-288-1266

[3]GeoForschungsZentrum Potsdam, Telegrafenberg, 14473 Potsdam, Germany: leni@gfz-potsdam.de, Fax: +49 -331-288-1349

Abstract

The passive margin of the South Atlantic shows typical features of a rifted volcanic continental margin, encompassing seaward dipping reflectors, continental flood basalts and high-velocity/density lower crust at the continent-ocean transition, probably emplaced during initial seafloor spreading in the Early Cretaceous.

The Springbok profile offshore western South Africa is a combined transect of reflection and refraction seismic data. This paper addresses the analysis of the seismic velocity structure in combination with gravity modelling and isostatic modelling to unravel the crustal structure of the passive continental margin from different perspectives.

The velocity modelling revealed a segmentation of the margin into three distinct parts of continental, transitional and oceanic crust. As observed at many volcanic margins, the lower crust is characterised by a zone of high velocities with up to 7.4 km/s. The conjunction with gravity modelling affirms the existence of this body and at the same time substantiated its high densities, found to be 3100 kg/m^3. Both approaches identified the body to have a thickness of about 10 km. Yet, the gravity modelling predicted the transition between the high-density body towards less dense material farther west than initially anticipated from velocity modelling and confirmed this density gradient to be a prerequisite to reproduce the observed gravity signal.

Finally, isostatic modelling was applied to predict average crustal densities if the margin was isostatically balanced. The results imply isostatic equilibrium over large parts of the profile, smaller deviations are supposed to be compensated regionally. The calculated load distribution along the profile implies that all pressures are hydrostatic beneath a depth of 45 km.

1. Introduction

The structure of the southwest African passive continental margin is still enigmatic as very little deep seismic data is available. We present the results of a combined on- and offshore seismic refraction experiment designed to image the deep structure of the margin. The resultant velocity-depth model is additionally constrained with free-air gravity data and finally used for isostatic calculations.

The investigated profile on- and offshore South Africa is located between the Orange River to the north and the Olifants River to the south (Fig. 1). The profile provides a transect through the westernmost Kalahari Shield, the southern edge of the Gariep Belt, the continental crust that has been stretched during the Mesozoic (>130 Ma) and the adjacent oceanic crust with cooling ages of ~130 Ma.

A special focus was set on the distribution of masses and on implications for the isostatic state of the system. 2D seismic raytracing yielded the velocity structure across the margin that was further constrained by gravity modelling especially where the seismic data quality was only moderate. Finally, isostatic modelling assuming local isostasy was used to evaluate the isostatic state of the margin. We explore how far the results from velocity, gravity and isostatic modelling are consistent and to what extent these findings provide information on the crustal structure of the margin.

2. Geological setting

The Springbok profile is 500 km long and crosses the western margin of the Republic of South Africa (R.S.A.) at 31°S. In the offshore part the profile starts at 3600 m water depth and runs through the central part of the Orange Basin in the shelf region (Fig.1). Near the shoreline the foothills of the deeply eroded, coast-parallel Panafrican Gariep Belt are crossed and the profile extends 100 km on land, where the topography is elevated to a maximum of 1000 m. At the landward termination of the Springbok profile the new study can be compared with the results of Green and Durrheim (1990) in which a refraction seismic experiment was carried out to study the deep crustal structure of the South African continent in the region of the Kalahari Shield. The latter formed when ocean-like crust was emplaced over the Kaapvaal Craton and its surrounding mobile belts. This stabilized the belt systems against the craton approximately 1 Ga ago (Eglington and Armstrong, 2003).

Subsequent, in the Damara orogeny a large network of Proterozoic to early Paleozoic orogenic belts developed through accretion coeval to the construction of Gondwana which surrounds and welds together the older Congo, Angola, and Kalahari Cratons (e.g. Grunow et al., 1996). In western Gondwana this belt system comprises the Kaoko, Damara, Gariep, and Saldanha Mobile Belts that have their equivalents on the South American side, e.g. the Ribeira Belt (Porada, 1979).

The Damara Belt, and its coast-parallel extension, the Kaoko and Gariep Belt underlie the passive margin offshore Namibia.

The Gariep Belt is restricted to the coast in southern Namibia and northern South Africa and is the only orogenic belt in which oceanic crustal material has been described. Metasedimentary sequences similar to the Damara Belt sequences represent continental rift conditions whereas the western units, separated by a suture zone, comprise metabasalts (Frimmel and Frank, 1998).

The Damara Orogeny was succeeded by a tectonically tranquil period, dominated by erosional and sedimentary processes until the opening of the South Atlantic in Early Cretaceous times around 136 Ma (Brown et al., 1995; Reeves and de Wit, 2000; Macdonald et al., 2003;). The continental break-up of Africa and South America was accompanied by massive, transient volcanic activity, which resulted in the emplacement of the Cretaceous igneous intrusions also called the South Atlantic Large Igneous Province. This Province encompasses the Paraná-Etendeka continental flood basalts and the offshore counterpart of extrusive complexes represented by a wedge of seaward-dipping reflectors (Hinz, 1981; Gladczenko et al., 1997; Talwani and Abreu, 2000; Bauer et al., 2000). Magmatic activity is attributed to the Tristan da Cunha hotspot activity and the emplacement of the seaward-dipping reflector wedge is supposed to be generated by a transient magmatic pulse (Gladczenko et al., 1997). The Etendeka Province is exposed onshore as eroded remnants of thick basaltic sequences, intrusive subhorizontal dolerite sills and a number of large subvolcanic ring intrusions, as the Damaraland Complexes (Milner et al., 1995, Trumbull et al., 2000). These ring complexes represent the eroded roots of ancient volcanoes, which were active

during flood volcanism (Marsh et al., 2001). South of the Walvis Ridge, offshore Namibia and R.S.A. several Late Mesozoic basins are present as the Walvis Basin, Luderitz Basin and Orange Basin that cumulated some kilometres of post break-up sediments.

The post break-up Orange Basin overlies basins of Early Cretaceous age that developed during several rift-stages prior and during the break-up of the South Atlantic Ocean. To the north the Orange Basin is bound by the Kudu arch and by the Agulhas-Columbine arch to the south (Muntingh and Brown, 1993). Post-rift sedimentary successions outline the basin, which had its main depocenter offshore Namaqualand south of the present day Orange River mouth since the drift-onset.

The underlying syn-rift successions are generally isolated grabens and half-grabens that trend approximately parallel to the present-day margin. Graben infill consists predominantly of Upper Jurassic and Lower Cretaceous coarse continental clastics, fluvial/lacustrine sediments and volcanic rocks of variable thickness (Muntingh and Brown, 1993).

3.1 Springbok seismic experiment

In April-May 2003 a geophysical experiment was carried out to study the shallow to deep crustal structure of the western margin of the Republic of South Africa (R.S.A.). The project was initiated by a German-South African consortium consisting of the GeoForschungsZentrum Potsdam (Germany), the Bundesanstalt fuer Geowissenschaften und Rohstoffe Hannover (Germany), and the Council for Geoscience (R.S.A.). The campaign included reflection and refraction seismic profiling offshore and partly onshore, where traverses have been surveyed parallel and perpendicular to the ocean-continent transition zone (Mahanyele et al., 2004; Schnabel et al., 2006). In this paper, the data from the Springbok profile (Fig. 2) are used to determine the seismic velocity structure of the crust along the transect. This information forms the starting point for the gravity modelling described in the subsequent sections 4.2 and 4.3.

Wide-angle reflection/refraction seismic data were collected by 5 ocean bottom hydrophones (OBH) and 40 seismometers (3-component, 1 Hz) onshore (Fig. 1b). Air-gun shots (volume ca. 70 l) were fired every 175 m generating signals that could be recorded at a maximum distance of 250 km. Additionally, three bore-hole shots were executed on land. Multichannel seismic (MCS) data have been collected along the offshore part of the Springbok profile to provide structural, reflection seismic images across the margin. For the purpose of the velocity

modelling presented in this paper, these data were included in that the geometry of the major sedimentary layers could be interpolated between the regions covered by the OBH data.

3.2 Velocity modelling

To determine the velocity model across the continental margin modelling based on travel time data was carried out by the use of the forward and inverse modelling package RAYINVR (Zelt and Smith, 1992). The data were analysed in the common receiver domain. Initial processing included band pass filtering, deconvolution, and frequency-wavenumber filtering. Travel times of reflected and refracted phases were determined and used as input information for the subsequent velocity modelling. Forward modelling with 2-D ray tracing was applied. Subsequently, the model was further updated by the use of damped least squares inversion. This procedure was applied to parts of the model with high ray coverage. Reflected events with limited lateral extension were modelled as floating reflector features. In other words, those boundaries (reflection segments) were established in the model which are not associated with a change in seismic velocity. Considering the general objective of this procedure, this ray-based modelling is comparable with pre-stack migration of seismic reflections, without obtaining the resolution and accuracy of the latter method.

Examples of the data and the ray tracing along the profile are shown in Figures 2-4. The data collected by OBH 1, located in the oceanic part of the profile, are displayed in the upper panel of Figure 2a. At the offset range of +- 75 km several phases with apparent velocities between 2.0 and 6.2 km/s are identified and picked (middle panel in Fig. 2b). The ray tracing demonstrates the coverage of the model around the OBH location (lower panel in Fig. 2c). The arrivals P2, P3, and P4 correspond to the marine sedimentary layers 2, 3, and 4 with velocities of 1.8, 2.4, and 3.2 km/s. The boundary underneath this package is also associated with a prominent reflection (P4P) that corresponds to the seismic basement. The crustal section underneath is divided into 3 layers with velocities from top to bottom of 4.7, 6.0 and 7 km/s, respectively. Moho reflections PmP can be identified that are reflected at 12 to 15 km depth.

An example for the modelling of the transitional crust is shown for OBH 2 (Fig. 3). For the upper sedimentary section, seismic phases P2, P3, and P4 are used to model layers 2, 3, and 4 with velocities of 1.8, 2.4, and 3.1 km/s, very similar to the modelling of the OBH 1 data shown in Figure 2. The seismic basement is associated with the boundary between layers 4 and 5. In contrast to OBH 1, the wide-angle reflection from this boundary (P4P) is less pronounced. The upper basement layer 5 is characterised by velocities of 5.1 km/s, which is slightly higher than at OBH 1 (4.7 km/s). Layer 6 shows a slight landward increase in velocity and thickness comparing OHB 1 and 2. An additional lower crustal body 7 was modelled landward of 110 km profile distance with velocities between 7.3 and

7.4 km/s. The top of this body is associated with the wide-angle reflections P7P. The depth of this boundary varies between 17 km at 110 km and 21 km at 200 km profile distance. The Moho depth was modelled with PmP wide-angle reflections and increased from 18 km at 110 km to 26 km at 200 km profile distance.

Figure 4 shows data and the corresponding ray tracing for land station 3 (location indicated in Figure 1). The smallest offsets of 21 km correspond to the distance of the seismometer on land to the air-gun location nearest to the coast. Upper crustal refracted arrivals P6 are identified and were modelled with velocities between 5.9 km/s surface and 6.3-6.5 km/s in the middle crust. Lower crustal velocities of 6.7 to 7.0 km/s were determined by the use of PmP reflected arrivals. The events named Pc1P and Pc2P were modelled as floating reflector segments which are not associated with a change of velocity at these boundaries. However, the location of these segments appears to be related with large velocity anomalies in the middle and lower crust in those regions.

Ray path coverage provides a measure for the resolution of the model along the profile (Fig. 5) and the derived final velocity model is shown in Figure 6. The offshore section is characterised by a sedimentary succession of 3 distinct layers with velocities of 1.8, 2.4, and 3.0-3.5 km/s. The sediments diminish to a thickness of a few hundred metres landward of the shelf break. Onshore, velocities of 6.0 km/s at the surface indicate that there is no sedimentary section in this region. Similar observations were reported by Green and Durrheim (1990). This is most likely related to the fact that inversion and erosion occurred at least since the

Tertiary in this area (Doucouré and de Wit, 2003) and led to exposure of crystalline rocks at present. The crustal structure along the profile can be divided into 3 major sections: (1) Normal oceanic crust can be identified at distances between 0 and 50 km. The crust shows a typical structure with velocities of 4.5-5.0 km/s and 6.2 km/s corresponding to the extrusive flows and sheeted dikes (layer 2A and 2B) and a layer with velocities of 7 km/s corresponding to the gabbroic layer 3 (e.g. Spudich and Orcutt, 1980; Pluijm and Marshak, 2004; Raum et al., 2006). (2) Transitional crust is encountered at distances between km 50 and km 250. The high velocities of 6.9 – 7.4 km/s found in the middle and lower crust in this region are a typical feature of rifted volcanic margins. Such high crustal velocities are commonly interpreted as heavily intruded crust in a developing continental rift and underplated bodies resulting from enhanced decompressional melting by mantle upwelling (e.g. White and McKenzie, 1989; Mjelde et al.; 2002; Raum et al., 2006). Following the interpretation of MCS reflection seismic data, this section is overlain by successions of volcanic flows and sediments forming the typical extrusive counterpart of the igneous crust at volcanic rifted margins (Talwani and Abreu, 2000, Schnabel et al., 2006). (3) Continental crust is modelled at distances between 250-300 and 500 km. The data provide no constraints to divide the crustal section into upper and lower crust in terms of a distinct velocity contrast but indicate a continuous increase of velocity between both layers. The crustal velocities vary between 5.9-6.1 km/s at the surface and 6.7-7.0 km/s at the Moho boundary. The inversion of P6 and PmP travel times revealed features of

increased velocities in the middle and lower crust in the coastal region less than 50 km wide. Ray-based modelling of reflected events showed that these regions with high velocities are associated with prominent wide-angle reflections.

The final velocity model was used to calculate an initial density model using well-established velocity-density relationships as described in subsequent section 4.2. From this point the model was calibrated with free-air gravity data to cross-check the results of the velocity modelling.

4.1. Gravity field

Figure 7 shows the marine free-air gravity anomaly across the study area which was extracted from Sandwell and Smith (1997) using the 1-min grid. Nearby the border from South Africa to Namibia, the marine gravity field is dominated by the so called "edge-effect" anomaly (Fig. 7). This feature is an elongated positive, free-air anomaly and is commonly observed at passive continental margins (Watts and Fairhead, 1999). The gravity anomaly has its maximum above the shelf break and trends parallel to the margin although with a variation in wavelength and amplitude.

Farther offshore a second positive anomaly (Fig. 7) was identified by Bauer et al. (2000). This feature is most pronounced between 27°S and 33°S although to the north it becomes less distinct and vanishes southwards of the mentioned range. The amplitude of this outer high is less than the amplitude of the prominent edge-effect high as it reaches only up to 20 mGal. Following the modelling of this study

this feature appears to be related to the change from normal oceanic crust to transitional crust.

In many cases an adjacent low occurs on the slope and rise of passive margins and sometimes an additional low emerges landward of the maximum. Along the Springbok profile the wavelength of the edge-effect anomaly reaches about 100 km, whereas immediately to the north the wavelength is reduced to less than 75 km. Farther north the anomaly widens again to more than 150 km. The amplitude also changes: in the north of the shown gravity map, where the Orange River drains into the ocean, a pronounced gravity signal of 60 mGal can be seen. Offshore the Olifants river mouth the same intensity is observed. Yet in general the magnitude of the signal is ~40 mGal along the margin.

Sleep and Fuyita (1997) propose a model to explain the edge-effect anomaly. This model consisted of an idealised transition between thick continental and thinner oceanic crust. However, Walcott (1972) and Watts (1988) demonstrated the importance of geologic processes and regional compensation. Watts (1988) distinguished between a rifting anomaly and a sedimentation anomaly. The first one results from the gravity response of the crystalline crust of the margin geometry through its evolution and the latter shows the influence of sedimentation on the margin. Accordingly, stretched crust produces a typical edge-effect anomaly prior to loading and is overlain by the sediment anomaly which is a high flanked by lows. Here, we explore how far the edge-effect is related to deep crustal heterogeneities.

4.2. Gravity modelling

As stated above the processing of the seismic refraction line Springbok revealed the velocity structure of the crust across the margin. However, as the data quality is minor in the middle shelf domain than in other domains further constraints on the crustal structure of the margin are needed. We tried to obtain further constraints by performing gravity modelling using seismic velocity results.

As a first step one gravity response of a density model derived from a velocity model was calculated. Therefore, the velocity model was converted into a density model. The respective density grid was obtained from the conversion of P-wave velocities to densities using the conversion function shown in Figure 8. This function integrates a compilation of global sample sets and is characterised by two correlations. The first correlation is for the P-wave velocity conversion for sedimentary rocks, the so called Nafe-Drake curve (Ludwig et al., 1970). The second correlation relates velocities and densities for igneous and metamorphic rocks (Christensen and Mooney, 1995).

The calculated density grid was used to set up the first gravity model along the profile. Crustal thickness is about 33 km beneath the continent and thins toward the ocean to less than 15 km. Density contours of every 50 kg/m³ were extracted from the grid and were adopted as body boundaries in the initial gravity model. Therefore, the respective gravity model consisted of 18 bodies. The densities of these bodies range from 1600 kg/m³ in the uppermost part of the model to

3300 kg/m³ in the mantle. This density converted structure of the velocity model was included into a gravity modelling programme and the gravity response of this model was calculated. Later, the geometry of this model was altered in order to gain a fit with the observed gravity field.

Gravity modelling was carried out with the programme IGMAS, which is an interactive, graphical computer system for the interpretation of potential field data in 3D (Götze and Lahmeyer, 1988). Geological structures are defined as polygons along parallel working planes. Between individual planes triangulations are calculated automatically.

Since the Springbok profile is just a single line and due to the lack of further information from the surrounding area, the geometry of the Springbok line was interpolated to 2 sections parallel to the original profile to prevent edge-effects within the modelling. The distance between the Springbok line and the adjacent profiles is 25 km. Additionally, 2 further sections are placed at 500 km distance for the same reason.

4.3. Initial gravity model

The gravity response of the initial density model which was derived from the velocity model is shown in Figure 9. In the oceanward part of the profile (up to kilometre 200) a reasonable fit between the measured and calculated gravity response of the initial gravity model is achieved. Yet a clear mass excess occurs across the middle shelf domain towards the continent resulting in an anomaly of

significant width and amplitude exceeding the properties of the edge-effect anomaly in terms of amplitude and wavelength. Moreover the position of the calculated maximum gravity response is offset eastward of the observed anomaly. To achieve a better consistency between the calculated gravity response and the observations the amplitude as well as the wavelength needed to be reduced.

Even though the velocity-density-conversion allows a range of densities for the respective velocity, a fit could not be obtained alone by changing the densities along the profile. The geometry of the model needed to be altered to yield a fit with the observations (Fig. 10). Several modelling attempts of changing the geometry of the crustal bodies were made, but resulted in very similar configurations to that of the final geometry of the model. These configurations involved the implementation of an additional less dense body in the upper crust (Fig. 10) with a density of 2620 kg/m^3. This body is not characterised by a strong velocity gradient observed in the seismic; but the velocity conversion allows a range of appropriate densities. Therefore the additional body of 2620 kg/m^3 is reasonable.

In order to improve the fit of the model diverse changes have been applied to it. The most significant change to the initial model was the westward shift of the transition between bodies of relatively high density towards less dense bodies in the mid-lower crust to account for the large wavelength of the calculated anomaly. In this domain the position of the Moho was deepened to reproduce the observed decrease of the amplitude. Furthermore, bodies of relative high

densities (densities of 2910 and 3100 kg/m^3, Fig.10) were reduced in dimension in comparison to less dense bodies (densities of 2720 and 2850 kg/m^3, Fig. 10) that were enlarged to diminish the amplitude.

There is no uniqueness in our final model configuration. It represents one solution amongst a lot of possibilities. However, we favour this final model because of it's alikeness to seismic geometries and properties.

5.1. Isostasy

The final gravity model which explains best the observed gravity helped us to derive the density structure of the crust and the depth to Moho across the margin. It was possible to reduce the degree of uncertainty concerning parts of the crustal structure derived from seismic data. As a next step we revised this model isostatically to analyse the present day state of the margin.

Isostasy describes the hydrostatic equilibrium of the earth's crust/lithosphere, obeying the principles of Archimedes. The principle of local isostasy is a 1D approach that assumes all loads to be compensated locally and surrounding loads are irrelevant to the isostatic response. Mass excesses in topography in the continental domain and mass deficiency in the oceanic domain are balanced by compensation masses. Isostasy requires the surface layers of the earth to be rigid and to "float" on, or in, a denser substratum representing the boundary between the lithosphere and the asthenosphere. Within these models the depth of compensation describes a depth, beneath of which all pressures are hydrostatic.

Density compensation as required by isostasy can be accomplished in several ways: Airy (1855) compensation is achieved by depressing /deflecting the Moho as a consequence of topographic loading (ρ_{crust} and ρ_{mantle} are treated as homogeneous); isostatic equilibrium is achieved by mountains having deep roots. Loading at the surface and subsequent deflection of the asthenosphere/lithosphere boundary deflects the crust-mantle boundary (Moho). The depth of compensation is arbitrary, but deeper than the deepest mountain root.

Whilst Airy´s concept is achieving isostatic compensation by deflecting the Moho and treats the density distribution as fixed, Pratt's concept (1855) uses horizontal variations in density over a prescribed (Moho) depth. Therefore, isostatic equilibrium is achieved by a variable crustal density which is related to the elevation above sea level. In our approach, modelling is based on the comparison of a reference model to a structural model, which is in this case the structure of the Springbok profile. The reference model represents a standard crustal block floating in or on the mantle. The block has a thickness h_c and a density ρ_c. The upper edge of the block is consistent with sea level, whereupon the compensation depth specifies the depth to which the body sinks into the mantle. In other words the compensation depth describes the thickness of this standard crustal block. At the lower edge of the block equation 1 is satisfied.

$$\rho_c h_c = \rho_M h_M \tag{1}$$

Where

ρ_c = crustal density; h_c = thickness of the crust;

ρ_M = mantle density; h_M = thickness of displaced mantle.

It is possible to calculate the amount of displaced mantle material for a given crustal thickness and respective densities. Within the reference model the average crustal density, the mantle density and the depth of compensation is prescribed.

For the structural model equation 2 is accomplished:

$$\rho_c \cdot h_c + \rho_M \cdot h_M = \rho_W \cdot h_W + \sum \rho_S \cdot h_S + \rho_C \cdot h_C + \rho_M \cdot h_M \qquad (2)$$

Where

ρ_c = crustal density; h_c = thickness of the crust;

ρ_M = mantle density; h_M = thickness of displaced mantle;

ρ_w = water density; h_w = water depth;

ρ_s = sediment density; h_s = thickness of the sediments.

Obeying Airy´s concept, the depth position of the Moho is calculated from equation 2. Based on Pratt's isostasy in turn the crustal density is achieved from equation 2 (e.g. Turcotte and Schubert, 2002, Fowler, 1996).

Isostatic modelling was done with the software Geological Modelling System (GMS) developed at the GeoForschungsZentrum Potsdam (Scheck and Bayer, 1999). This programme allows multi 1D isostatic calculation for a 3D grid.

5.2. Isostatic model

The structure of the density model down to a depth of ~7 km was used as input for the isostatic modelling (Fig. 11a). This boundary is defined as a density contrast between densities < 2700 kg/m³ and densities > 2700 kg/m³, which refers to a velocity increase to > 6 km/s. The position of the Moho was known from seismic and gravity modelling and used here as the lower boundary for a Pratt model. We used this model to obtain the lateral variation in average crustal density below the 6 km/s iso-velocity level.

A density distribution was calculated for the mid to lower crust according to Pratt to achieve isostatic compensation over the prescribed Moho depth (Fig. 11b). Several reference models had been tested. The reference model reproducing the densities derived from gravity modelling best had an average crustal density of 2965 kg/m³ and a compensation depth of 43 km.

The results of the isostatic modelling are shown in Figure 11.

Panel a shows the density distribution in the gravity model and the depth interval which was used for isostatic modelling outlined in black. Panel b images the calculated Pratt density distribution along the profile derived from isostatic modelling. Whereas, panel c shows the results of the isostatic modelling in comparison to the average density of the gravity model for the respective depth interval.

Isostatic modelling revealed a density range for the middle and lower crust varying between 2760 and 3050 kg/m³. In the middle of the profile (between km 80 and km 250) the densities of the Pratt model are in good agreement with

the densities in the gravity model (Fig. 11c). To both sides of this part the differences between both models increase and the predicted densities are higher than the ones modelled with gravity. But close to the coast the trend reverses and the isostatically predicted densities are lower than seen in the gravity model.

6. Discussion

6.1 Crustal structure at Springbok and along the margin

The velocity distribution obtained by 2D velocity modelling allows the following interpretation of the margin (Fig. 12): On top of the section velocity modelling revealed a sedimentary succession of considerable thickness of about 4-5 km, which diminishes towards the continent until the thickness is reduced to a few hundred metres landward of the shelf break and finally vanishes onshore. Between km 0 and km 50 velocity contrasts within the crust separate oceanic layers 2A and 2B. Layer 2A is commonly interpreted as extrusive flows of pillow basalts with velocities of 4.5-5.0 km/s and layer 2B as basaltic sheeted dikes with velocities of 6.2 km/s. Beneath of which the velocities increase to 7 km/s which indicates the gabbroic layer 3. This layer is in turn underlain by a layer of cumulates, rocks formed from mafic minerals in a cooling magma (e.g. Spudich and Orcutt, 1980; Pluijm and Marshak, 2004; Raum et al., 2006).

Transitional crust has been identified from km 50 to km 250 along the profile where the middle and lower crust is characterised by high P-wave velocities (6.9 – 7.4 km/s) as most commonly observed at rifted volcanic margins.

Heavily intruded continental crust or mafic intrusions/underplating are commonly interpreted to cause these high velocities in the respective depth range but from seismic resolution alone it is not possible to distinguish between both. It is very likely that the interpreted transitional upper crust is a mixture of both and includes extended and rifted old continental segments. On top of this section, seaward dipping reflectors are observed in MCS which are interpreted to represent volcanic flows and sediments (Talwani and Abreu, 2000, Schnabel et al., 2006) most likely emplaced during continental break-up and early seafloor spreading (e.g. Eldholm et al., 1995). Thirdly, from km 250-300 to km 500 velocities range from 5.9 to 6.1 km/s at surface and thus indicate continental crust. Here, the crust is characterised by a continuous velocity increase with depth, but no significant velocity contrasts were found to divide the crust into an upper and a lower continental crust. Within the continental crust small scale zones of high velocities are spatially linked with the location of the Gariep Mobile Belt. The latter could either represent minor intrusions related to the continental break-up or relicts of high grade metamorphic rocks formed during the Damara Orogeny.

In comparison to this fairly small scale local features, lower crustal bodies of high seismic velocities and also high densities of considerably extension as observed along the Springbok line have been documented on several other volcanic margins, although their origin remains controversial. Talwani and Abreu (2000) demonstrated the presence of such bodies characterised by high seismic velocities (7.2-7.4 km/s) both in the North Atlantic offshore of the eastern United States and

in the South Atlantic offshore Brazil and Namibia. These bodies reach up to 24 km in thickness and are interpreted to originate from accretion processes of igneous material during the break-up (Holbrook et al., 1994). Furthermore, these high-velocity bodies correlate spatially with break-up features as defined by Eldholm et al. (1995) including onshore continental flood basalts, extrusive basaltic complexes along the continent-ocean transition and the occurrence of seaward dipping reflector wedges.

To explain the evolution of passive margins one can not ignore the very first, but elegant theory of basin evolution by McKenzie (1978). He developed a concept of basin evolution that included the thinning of the lithosphere accompanied by asthenospheric upwelling to maintain the isostatic equilibrium. Later, authors elaborated on McKenzie´s model by proposing a passive upwelling of the asthenosphere to result in melt generation (Foucher et al., 1982). White and McKenzie (1989) developed the discussion further by suggesting that decompressional melting just occurs if a mantle plume causes a thermal anomaly to create large quantities of melts.

On the other hand numerical simulations showed an alternative of mechanical processes generating melt volumes (Gernigon et al., 2004). Due to crustal thinning mantle material rises and consequently decompressional melting processes in the head of the rising material cause significant volumes of melt (van Wijk et al., 2001). In these models the volume of melt is controlled by the thinning factor beta.

The volcanic character of the South Atlantic margin south of the Walvis Ridge-Rio Grande Rise appears to be independent from plume influence, an interpretation also suggested by the presence of a wedge of seaward dipping reflectors. This wedge occurs along the entire margin south of the Walvis Ridge and is constant in width and volume (Talwani and Abreu, 2000). North of the hotspot traces of the Walvis Ridge and the Rio Grande Rise these seaward dipping reflectors vanish and continental flood basalts are not observed. The Walvis Ridge separates the southern part of the margin which is volcanic in nature from the northern part where the margins appears to non-volcanic in character (e.g. Gladczenko et al., 1998).

The involvement of a mantle plume is not a prerequisite to produce melts but increases the generated melt volumes and influences the melt composition. In the plume vicinity melts are rich in magnesium due to increased mantle temperatures which results in increased seismic velocities compared to velocities of rocks originating from melts generated distal to a plume head (White and McKenzie, 1989, Holbrook and Kelemen, 1993). Studies undertaken by Trumbull et al. (2000, 2002) argue for the influence of a mantle plume as far south as offshore Namibia. Farther south they propose a diminishing influence of the Tristan da Cunha plume based on decreasing magnesium composition in the crust.

North of our studied profile the MAMBA experiments offshore Namibia (Bauer et al., 2000) aimed to reveal the crustal structure of the margin with a combined

approach of seismic interpretation and gravity modelling. In particular, these results indicate the presence of lower crustal bodies characterised by P-wave velocities >7 km/s and densities >3000 kg/m³. According to these data, the gravity observations are explained by a superposition of topographic effects and lateral density variations, but, like along the Springbok profile lower crustal bodies of high densities are required in addition.

Comparing the results of the three seismic refraction experiments it becomes clear that the thickness and the average velocities of the lower crustal body decrease from north to south (Fig. 13). Accordingly, the 3D nature of this high-velocity body is not debatable. It is characterised by a southwards decreasing thickness but also a slight decrease in maximum velocities. The MAMBA profiles reveal a high-velocity body with a thickness of ~20 km and with velocities of up to 7.6 km/s. Along the Springbok transect our seismic velocity modelling results reveal a P-wave velocity of 7.4 km/s and a maximum thickness of 10 km for this body. This confirms the tendency that the dimension of the high-velocity body diminishes from north to south. These observations appear to support the suggestions of Trumbull et al. (in press), who argue for a reduced magnesium content in the produced melts from north to south. Furthermore, this aligns with the theory of less melt production distal to mantle plumes.

A further seismic refraction/reflection line (Profile 95303) offshore the Orange River mouth identified a similar crustal structure across the margin, including a high-velocity body (7.1-7.4 km/s) in the lower crust (Schinkel, 2006). Gravity

modelling suggests that this body has a density of 3130 kg/m^3 and has a maximum thickness of about 13 km. In this study, the interpretation of mafic intrusions in the lower crust have been emplaced in late rift stages is favoured to explain the presence of the lower crustal body.

A further seismic refraction/reflection line (Profile 95303) offshore the Orange River mouth identified a similar crustal structure across the margin, including a high-velocity body (7.1-7.4 km/s) in the lower crust (Schinkel, 2006). Gravity modelling suggests that this body has a density of 3130 kg/m^3 and has a maximum thickness of about 13 km. In this study, the interpretation of mafic intrusions in the lower crust that have been emplaced in late rift stages is favoured to explain the presence of the lower crustal body.

6.2. Gravity anomalies along the margin

The final density model reproduces the observed edge-effect anomaly. The maximum of the calculated gravity anomaly is located above the shelf break which coincides with the position of a lateral density gradient from dense to less dense material in the lower crust. This density contrast in the lower crust is crucial to reproduce the observed edge-effect anomaly. In comparison to the initial velocity model this gradient had to be dislocated oceanward and amplified. The areas of high densities still correlate spatially with zones of high velocities

and reach a maximum thickness of 10 km. Isostatic modelling also confirms high densities within this domain of the margin.

Thus in summary, the edge-effect anomaly is a superposition of two components. Firstly, a sediment pile on top of the model produces a rise of the observed gravity curve. This, however, does not reproduce the observed gravity pattern. So secondly, a high-density body in the lower crust is required to produce a density contrast which in turn causes the anomaly to decline continentward and follow the observed curve.

Offshore Namibia Stewart et al. (2000) modelled the gravity low on the shelf landward of the gravity high with a sediment filled graben structure. Due to the fact that no considerable sediment-filled graben structure is observed in MCS, we argue for the density gradient in the lower crust to force the amplitude to decline.

An earlier gravity study offshore Namibia (Light et al., 1992) was performed to image the deep crustal structure that infers the presence of an anomalous high-density body in the lower crust, which was interpreted as a continuous mantle wedge. In contrast to this interpretation our findings suggest P-wave velocities and densities higher than expected for normal crust but lower than for mantle properties. In addition the spatial distribution of the properties constrains the geometry of the high-velocity body and excludes a mantle wedge

Furthermore in the southern Orange Basin 3D gravity modelling revealed a similar crustal structure as derived from the Springbok profile and indicates the presence of a high-density body in the lower crust which is about 11 km thick in

average, and has a density of 3200 kg/m³ (Hirsch et al., in press). There it was shown that the gravity signal caused by the sedimentary wedge on top of the model and the lower crustal bodies act in concert to reproduce the observed edge-effect anomaly.

6.3. Consideration of isostasy

The results of isostatic modelling imply isostatic equilibrium for the high-density body in the lower crust over large parts. This is concluded from the consistence between the lower crustal densities obtained by isostatic and by gravity modelling. Deviations from isostasy are less than 50 km wide and are probably compensated regionally.

For the isostatic modelling a series of reference models have been tested. The fit between the isostatically obtained densities and the average density of the gravity model could also be achieved using different reference models. A reduction of the compensation depth in combination with a reduced average crustal density results in the same density distribution as if a reference model with a deeper compensation depth was used in combination with higher average crustal density. For a minimum compensation depth of 40 km the respective reference density is 2900 kg/m³. This value represents a reasonable average of continental and oceanic crustal density. A shallower compensation depth is impossible due to the thickness of the unstretched continental crust. To increase the compensation depth to 45 km demands a crustal reference density of 2980 kg/m³ which is a

rather high value for average density between oceanic and continental crust. Nevertheless, all these tests provide reasonable density variations for the continental crust ranging from 2800 to 3000 kg/m³. Thus we conclude that the system is isostatically balanced at the depth level of 40-45 km and at least at 45 km depth all pressures are hydrostatic.

The gravity modelling of the initial model configuration revealed a mass excess in the range from km 200 to km 350, which does not reproduce the observations. To obtain a better fit this mass excess was reduced in wavelength and amplitude. In contrast, local isostatic modelling predicted higher densities than derived by gravity modelling in the 260-300 km segment of the profile. These higher densities in the crust predicted by local isostasy are contradictory to the results of the gravity modelling. Obviously the respective segment of the profile is less dense than isostatically required and indicates an isostatic disturbance at this location. Here the load is not equilibrated locally, but appears to be sustained by the regional rigidity of the lithosphere. It is very likely that crustal blocks are not completely compensated in terms of local isostasy. The principle of Pratt's isostasy assumes all loads to be compensated locally which is equivalent to the assumption of no elastic strength in the lithosphere (Roberts et al., 1998). This assumption is of course not correct and may lead to overestimates of the average crustal density in the calculations because loads are distributed regionally.

In contrast to our results along Springbok, farther south isostatic models suggest that the margin there is rather far from isostatic equilibrium (Hirsch et al. in

press). Isostatic and gravity analysis based on a 3D structural model of the Orange Basin revealed a large discrepancy between crustal configurations predicted by local isostasy and 3D gravity modelling. There, however, deep seismic constraints are missing.

7. Conclusions

Three types of models have been used to derive a comprehensive picture of the crustal structure of the South African passive continental margin. This conjunction of different approaches reduced the ambiguousness in both, the seismic velocity modelling and also the modelling of potential field data, which alone always leads to non unique results. To top the modelling off, isostatic modelling was applied to reveal the isostatic state of the margin.

From seismic modelling we identified three types of crustal structure along the transect. In the western domain of the profile typical oceanic layered crust where layer 2A, 2B and 3 are distinguished is followed eastward by a transitional crust in the middle domain of the profile. There typical volcanic margin features were found encompassing seaward dipping reflectors in the MCS data and a high-velocity, high-density body in the lower crust revealed by 2D seismic velocity modelling. Finally, continental crust was identified at the landward termination of the profile, where P-wave velocities imply the lack of a considerable sediment cover, but indicate the presence of a metasedimentary succession. In the middle

and lower continental crust some local anomalies of high velocity and density suggest minor, break-up related features.

The density structure of the margin was approved by gravity modelling which required a slight westward shift of the boundary between the transitional and the continental crust in comparison to the initial density model which was yielded from the velocity model using two conversion laws to account for the mass excess of the initial density model. Accordingly, the high-velocity body in the lower crust was modelled with a density of 3100 kg/m^3.

Isostatic modelling indicates that the isostatic equilibrium is established over large parts of the profile. The best-fit and most reasonable isostatic model included an average reference crustal density of 2965 kg/m^3 in combination with a compensation depth of 43 km. We found that all masses are balanced and pressures are hydrostatic at least below a depth of 45 km.

Acknowledgements

This work has been done in the framework of INKABA yeAFRICA at the GeoForschungsZentrum Potsdam.

We wish to thank Dieter Franke, Sönke Neben and Michael Schnabel from the BGR and in addition Trond Ryberg, Albrecht Schulze and Michael Weber from the GeoForschungsZentrum Potsdam for preparation and execution of the Springbok experiment. Geophysical Instrument Pool Potsdam (GIPP) provided

the instruments for the onshore part of the experiment. Thanks go also to the field crews on- and offshore for their work during the measurements and in particular to Coenie de Beer for the preparation of the experiments. J. Mahayele is acknowledged for his work in the first phase of data analysis. Special thanks go to J. Stankiewicz for his help to generate the geological map.

Isostatic modelling was performed with the Geological Modelling System (GMS) developed at the GeoForschungsZentrum Potsdam, Department Organic Geochemistry under the leadership of Prof. Dr. U. Bayer.

We thank H.-J. Götze and S. Schmidt, University of Kiel, for the 3D gravity modelling programme IGMAS.

Airy, G.B. (1855) On the Computation of the Effect of the Attraction of Mountain-Masses, as Disturbing the Apparent Astronomical Latitude of Stations in Geodetic Surveys. Philosophical Transactions of the Royal Society of London, 145: 101-104.

Bauer, K., Neben, S.,Schreckenberger, B.,Emmermann, R.,Hinz, K.,Fechner, N.,Gohl, K.,Schulze, A.,Trumbull, R. B., and Weber, K. (2000) Deep structure of the Namibia continental margin as derived from integrated geophysical studies. Journal of Geophysical Research, B, Solid Earth and Planets, 105(11): 25,829-25,853.

Brown, L.F., Jr., Benson, J.M., Brink, G.J., Doherty, S., Jollands, A., Jungslager, E.H.A., Keenan, J.H.G., Muntingh, A., and van Wyk, N.J.S. (1995) Sequence stratigraphy in offshore South African divergent basins: an atlas on exploration for Cretaceous lowstand traps by SOEKOR (Pty) Ltd. American Association of Petroleum Geologists, Studies in Geology, 41, 184 pp.

Christensen, N.I., and Mooney, W.D. (1995) Seismic velocity structure and composition of the continental crust: a global view. Journal of Geophysical Research, 100(B6): 9761-9788.

de Wit, M.J., and Stankiewicz, J. (2007) Restoring Pan African-Brasiliano connections: more Gondwana control, less Trans-Atlantic corruption. EGU 2007-A-06500, Vienna, Austria.

Doucoure, C.M., and de Wit, M.J. (2003) Old inherited origin for the present near-bimodal topography of Africa. Journal of African Earth Sciences, 36(4): 371-388.

Eglington, B.M., and Armstrong, R.A. (2003) Geochronological and isotopic constraints on the Mesoproterozoic Namaqua-Natal Belt; evidence from deep borehole intersections in South Africa. Precambrian Research, 125(3-4): 179-189.

Eldholm, O., Skogseid, J., Planke, S. and Gladczenko, T.P., 1995. Volcanic margin concepts. In: E. Banda, Talwani, M. & Torné, M. (Editor), Rifted Ocean–Continent Boundaries. Kluwer Academic Publishers, pp. 1-16.

Foucher, J.-P., Le Pichon, X. , Sibuet, J.-C., Roberts, D. G., Chenet, P.-Y., Bally, A. W., Oxburgh, E. R., Kent, P., Dewey, J. F.,Bott, M. H. P., Jackson, J. A., Osmaston, M. F. and Turcotte, D.L., 1982. The ocean-continent transition in the uniform lithospheric stretching model: Role of partial melting in the mantle. Philosophical Transactions of the Royal Society of London. Series A, Mathematical and Physical Sciences, The Evolution of Sedimentary Basins, 305(1489): 27-43.

Fowler, C.M.R., 1996. The Solid Earth: an introduction to global geophysics. Cambridge University Press, Cambridge, 704 pp.

Frimmel, H.E., and Frank, W. (1998) Neoproterozoic tectono-thermal evolution of the Gariep Belt and its basement, Namibia and South Africa. Precambrian Research, 90(1-2): 1-28.

Gernigon, L., Ringenbach, J.-C., Planke, S., and Le Gall, B. (2004) Deep structures and breakup along volcanic rifted margins: insights from integrated studies along the outer Voring Basin (Norway). Marine and Petroleum Geology, 21(3): 363-372.

Gladczenko, T.P., Hinz, K., Eldholm, O., Meyer, H., Neben, S., and Skogseid, J., 1997. South Atlantic volcanic margins. Journal of the Geological Society, 154(3): 465-470.

Gladczenko, T.P., Skogseid, J., and Eldholm, O. (1998) Namibia volcanic margin. Marine Geophysical Researches, 20(4): 313-341.

Götze, H.-J., and Lahmeyer, B. (1988) Application of three-dimensional interactive modeling in gravity and magnetics. Geophysics, 53(8): 1096-1108.

Green, R.W.E., and Durrheim, R.J. (1990) A seismic refraction investigation of the Namaqualand Metamorphic Complex, South Africa. Journal of Geophysical Research, 95(B12): 19,927-19,932.

Grunow, A., Hanson, R., and Wilson, T. (1996) Were aspects of Pan-African deformation linked to Iapetus opening? Geology, 24(12): 1063-1066.

Hinz, K. (1981) Hypothesis on terrestrial catastrophes: wedges of very thick oceanward dipping layers beneath passive continental margins - their origins and paleoenvironmental significance. Geologisches Jahrbuch, Series E, 22: 1-28.

Hirsch, K.K., Scheck-Wenderoth,M., Paton,D. A., and Bauer,K. , 2007. Crustal structure beneath the Orange Basin, South Africa South African Journal of Geology, 110(2/3): 249-260.

Holbrook, W.S., and Kelemen, P.B. (1993) Large igneous province on the US Atlantic margin and implications for magmatism during continental breakup. Nature (London), 364(6436): 433-436.

Holbrook, W.S., Reiter, E. C., Purdy, G. M., Sawyer, D., Stoffa, P. L., Austin Jr., J. A., Oh, J., and Makris, J. (1994) Deep structure of the U.S. Atlantic continental margin, offshore South Carolina, from coincident ocean bottom and multichannel seismic data. Journal of Geophysical Research, B, Solid Earth and Planets, 99(5): 9155-9178.

Light, M.P.R., Maslanyj, M.P. and Banks, N.L., 1992. New geophysical evidence for extensional tectonics on the divergent margin offshore Namibia. In: B.C. Storey, T. Alabaster and R.J. Pankhurst (Editors), Magmatism and the causes of continental break-up. Special Publications. Geological Society, London, United Kingdom, pp. 257-270.

Ludwig, W.J., Nafe, J.E. and Drake, C.L., 1970. Seismic refraction. In: A.E. Maxwell (Editor), The Sea. Wiley-Interscience, New York, pp. 53-84.

Macdonald, D., Gomez-Perez, I., Franzese, J., Spalletti, L., Lawver, L., Gahagan, L., Dalziel, I., Thomas, C., Trewin, N., Hole, M., and Paton, D. (2003) Mesozoic break-up of SW Gondwana; implications for regional

hydrocarbon potential of the southern South Atlantic. Marine and Petroleum Geology, 20(3-4): 287-308.

Mahanyele, P.J., Bauer, K., Franke, D., Schulze, A., Ryberg, T., De Beer, C. H.,Neben, S.,Schreckenberger, B., Stettler, E. H., and Weber, M.H., 2004. How far to the south does the volcanic margin of Southwest Africa extend? An initial velocity model for the ocean-continent transition in the southern Cape Basin, 64. Jahrestagung der Deutschen Geophysikalischen Gesellschaft. Abstract volume, Berlin, pp. 443-444.

Marsh, J.S., Ewart, A., Milner, S.C., Duncan, A.R., and Miller, R.M. (2001) The Etendeka igneous province; magma types and their stratigraphic distribution with implications for the evolution of the Parana-Etendeka flood basalt province. Bulletin of Volcanology, 62(6-7): 464-486.

McKenzie, D. (1978) Some remarks on the development of sedimentary basins. Earth and Planetary Science Letters, 40(1): 25-32.

Milner, S.C., LeReox, A.P. and O'Connor, M., 1995. Age of Mesozoic igneous rocks in northwestern Namibia, and their relationship to continental breakup. Journal of the Geological Society London, 152(1): 97-104.

Mjelde, R., Kasahara, J., Shimamura, H., Kamimura, A., Kanazawa, T., Kodaira, S., Raum, T., and Shiobara, H. (2002) Lower crustal seismic velocity-anomalies; magmatic underplating or serpentinized peridotite? Evidence from the Vøring Margin, NE Atlantic. Marine Geophysical Researches, 23(2): 169-183.

Muntingh, A. and Brown, L.F. Jr., 1993. Sequence stratigraphy of the petroleum plays, postrift Cretaceous rocks (lower Aptian to upper Maastrichtian), Orange Basin, western offshore, South Africa. In: P. Weimer, Posamentier, H.W. (Editor), Siliclastic Sequence Stratigraphy - recent developments and applications. American Association of Petroleum Geologists Memoir, Tulsa, pp. 71-97.

Pluijm, B.A.v.d. and Marshak, S., 2004. Earth Structure. W. W. Norton Company, New York, London, 656 pp.

Porada, H. (1979) The Damara-Ribeira orogen of the Pan-AfricanBrazilano cycle in Namibia (southwest Africa) and Brazil as interpreted in terms of continental collision. Tectonophysics, 57: 237-265.

Pratt, J.H. (1855) On the Attraction of the Himalaya Mountains, and of the Elevated Regions beyond Them, upon the Plumb-Line in India. Philosophical Transactions of the Royal Society of London, 145: 53-100.

Raum, T., Mjelde, R., Shimamura, H., Murai, Y., Brastein, E., Karpuz, R.M., Kravik, K., and Kolsto, H.J. (2006) Crustal structure and evolution of the southern Vøring Basin and Vøring Transform Margin, NE Atlantic. Tectonophysics, 415(1-4): 167-202.

Reeves, C., and de Wit, M. (2000) Making ends meet in Gondwana: retracing the transforms of the Indian Ocean and reconnecting continental shear zones. Terra Nova, 12(6): 272-280.

Roberts, A.M., Kusznir, N.J., Yielding, G., and Styles, P. (1998) 2D flexural backstripping of extensional basins; the need for a sideways glance. Petroleum Geoscience, 4(4): 327-338.

Sandwell, D.T. and Smith, W.H.F., 1997. Marine gravity anomaly from Geosat and ERS 1 satellite altimetry. Journal of Geophysical Research, B, Solid Earth and Planets, 102(5): 10,039-10,054.

Scheck, M. and Bayer, U., 1999. Evolution of the Northeast German Basin -- inferences from a 3D structural model and subsidence analysis. Tectonophysics, 313(1-2): 145-169.

Schinkel, J. (December 2006) Tiefenstruktur der Kontinent-Ozean-Grenze vor dem Orange Fluss, Namibia. Alfred-Wegener-Institute for polar and marine research. Institut für Geowissenschaften der Friedrich-Schiller-Universität, Jena.

Schnabel, M., Franke, D., Grassmann, S. , Neben, S., Damm, V., Pelliza, H., and Dos Santos,P. R. (2006) Deep Structure of the Argentine and Conjugated South African Continental Margins. AAPG International Conference and Exhibition, Perth, Australia.

Sleep, N.H. and Fuyita, K., 1997. Principles of Geophysics. Blackwell Science, Malden, 586 pp.

Spudich, P., and Orcutt, J. (1980) A New Look at the Seismic Velocity Structure of the Oceanic Crust. Reviews of Geophysics and Space Physics, 18(3): 627-645.

Stewart, J., Watts, A.B., and Bagguley, J.G. (2000) Three-dimensional subsidence analysis and gravity modelling of the continental margin offshore Namibia. Geophysical Journal International, 141(3): 724-746.

Talwani, M. and Abreu, V., 2000. Inferences regarding initiation of oceanic crust formation from the U.S. East Coast Margin and conjugate South Atlantic margins. In: W. Mohriac, Talwani, M. (Editor), Atlantic rifts and continental margins. American Geophysical Union, Washington, DC, United States, pp. 211-233.

Trumbull, R.B., Reid, D.L., de Beer, C., vanAcken, D. and Romer, R.L., 2007. Magmatism and Continental Breakup at the West Margin of Southern Africa: A Geochemical Comparison of Dolerite Dikes from NW Namibia and the Western Cape. South African Journal of Geology, 110(2/3): 477-502.

Trumbull, R.B., Emmermann, R., Bühn, B., Gerstenberger, H., Mingram, B., Schmitt, A., and Volker, F. (2000) Insights on the genesis of the Cretaceous Damaraland igneous complexes in Namibia from a Nd- and Sr-isotopic perspective. Communications of the Geological Survey of Namibia, 12: 313-324.

Trumbull, R.B., Sobolev, S.V. and Bauer, K., 2002. Petrophysical modeling of high seismic velocity crust at the Namibian volcanic margin. In: M.A. Menzies, Klemperer, S.L., Ebinger, C.J., Baker, J. (Editor), Volcanic rift margins. Special Paper. Geological Society of America, Boulder, CO, United States, pp. 225-234.

Turcotte, D.L. and Schubert, G., 2002. Geodynamics. New York, NY (US) ;John Wiley and Sons, Inc., United States, 472 pp.

van Wijk, J.W., Huismans, R.S., ter Voorde, M., and Cloetingh, S.A.P.L. (2001) Melt generation at volcanic continental margins; no need for a mantle plume? Geophysical Research Letters, 28(20): 3995-3998.

Walcott, R.I. (1972) Gravity, Flexure, and the Growth of Sedimentary basins at a Continental Edge. Geological Society of America Bulletin, 83(6): 1845-1848.

Watts, A.B. (1988) Gravity anomalies, crustal structure and flexure of the lithosphere at the Baltimore Canyon Trough (Atlantic). Earth and Planetary Science Letters, 89(2): 221-238.

Watts, A.B. and Fairhead, J.D., 1999. A process-oriented approach to modeling the gravity signature of continental margins. The Leading Edge, 18: 258-263.

White, R., and McKenzie, D. (1989) Magmatism at rift zones - The generation of volcanic continental margins and flood basalts. Journal of Geophysical Research, 94(6): 7685-7729.

Zelt, C.A., and Smith, R.B. (1992) Seismic traveltime inversion for 2-D crustal velocity structure. Geophysical Journal International, 108: 16-34.

Fig. 1: (a) Simplified geology of southwestern Africa (modified after de Wit and Stankiewicz, 2007) including the old cratons and surrounding mobile belts which accreted during the Damara Orogeny. Along the Atlantic margin three major sedimentary basins are shown in combination with the location of the Springbok seismic refaction/reflection profile crossing the Kalahari Shield, running through the offshore Orange Basin and ending in approximately 3600 m water depth in the oceanward domain of the profile. Farther north are the positions of the MAMBA profiles given in red. (b) Bathymetric map (Sandwell and Smith, 1997) of the South African margin with the Springbok profile in red. Yellow circles indicate the positions of the OBHs offshore. 40 onshore receivers are plotted as red triangles, overlain by 3 stars indicating the position of the onshore borehole shots. An arrow indicates the position of land station 3. (c) Cross-section of the southwestern African continental margin illustrating the geometries of syn- and post-rift sequences within the Orange Basin (modified after Brown et al. 1995).

Fig. 2: (a) Receiver gather for OBH 1 from km 20 to km 160 along the Springbok profile. The vertical axis corresponds to reduced travel times (reduction velocity is 6 km/s). Distances represent the model coordinates along the profile and the grey circle indicates the position of OBH 1. (b) Observed and calculated travel times based on the final P-wave velocity model. The arrival P1 refers to the water wave, arrivals P2, P3 and P4 correspond to the marine sedimentary layers the base of which is a prominent reflection (P4P) that refers to the seismic basement. The underlying crust can be subdivided into 3 sections (P5, P6, P7) beneath this section the Moho reflection PmP can be identified. Pn - refracted wave from the upper oceanic mantle. (c) Model section showing ray paths for OBH 1.

Fig. 3: (a) Receiver gather for OBH 2 from km 70 to km 240 along the Springbok profile. The vertical axis corresponds to reduced travel times (reduction time is 6 km/s). Distances represent the model coordinates along the profile and the grey circle indicates the position of OBH 2. (b) Observed and calculated travel times

based on the final P-wave velocity model. The arrival P1 refers to the water wave, arrivals P2, P3 and P4 correspond to the marine sedimentary, P4P refers to the seismic basement. The underlying crust is divided into 4 layers based on the modelling of the refracted arrivals P5, P6, P7, and the P7P reflection arrivals. The latter corresponds to the reflection from top of the lowermost crustal body. Arrival PmP refers to the Moho reflection and Pn corresponds to a refracted wave from the upper oceanic mantle. (c) Model section showing ray paths for OBH 2.

Fig. 4: (a) Receiver gather for the onshore receiver station 3 (for location see Fig.1b). The smallest offsets of 21 km correspond to the distance of the seismometer on land to the air-gun location nearest to the coast. The vertical axis corresponds to reduced travel times (reduction velocity is 6 km/s) and the grey triangle indicates the position of land station 3. Distances represent the model coordinates along the profile. (b) Observed and calculated travel times based on the final P-wave velocity model. (c) Model section showing ray paths for land station 3.

Fig. 5: Figure of the ray paths in the model. (a) shows the ray paths for P3 and P4 which correspond to the marine sedimentary layers and also the P4P which corresponds to the seismic basement. Panel (b) shows the ray paths for P5, P6, P7, and P7P which travel through the mid to lower crust. Panel (c) images the ray paths for the modelled floating reflectors Pc1P and Pc2P. Panel (d) shows the ray paths for P8, PmP and Pn.

Fig. 6: Final velocity model, black lines indicate model boundaries. Between km 0 and km 50 the velocity distribution indicates typical oceanic crust, followed eastward by a zone of transitional crust and from km 275 on velocities of typical continental crust is modelled.

Fig. 7: Marine free-air gravity field with positive "edge-effect" anomaly (Sandwell and Smith, 1997). 2 dashed black lines mark the prominent edge-effect and the farther offshore a second minor feature here referred to as the "outer high". Both anomalies have also been identified along the MAMBA profile offshore Namibia (Bauer et al., 2000)

Fig. 8: Conversion function used to derive densities from P-wave velocities of the final velocity model according to experimental laws (Christensen and Mooney, 1995; Ludwig et al., 1970).

Fig. 9: Calculated and observed gravity curve (upper panel) shown for the initial gravity model (lower panel). The structure of the model is derived from the converted final velocity model shown in Fig. 6. The gravity response of this model implies a mass excess across the shelf break. Densities are given in kg/m^3 and the reference density is 3043 kg/m^3.

Fig. 10: The upper panel shows the calculated gravity response and the observed gravity for the final gravity model. This Final gravity model (lower panel) altered between km 250 and km 300 with respect to the initial density model derived from seismic velocity modelling and also the lower crustal body (ρ=3100 kg/m^3) is less dense than in the initial model (ρ=3150 kg/m^3). Densities are given in kg/m^3 and the reference density is 3043 kg/m^3.

Fig. 11: Isostatic modelling results. Panel (a) shows the final gravity model and the depth interval which was used in the isostatic modelling (outlined in black) to predict the average crustal density if the margin is in isostatic equilibrium. Panel (b) shows the average crustal densities derived from isostatic modelling for the respective depth interval. Panel (c) compares the average crustal densities from

isostatic modelling with the average crustal densities from gravity modelling for the same depth range.

Fig. 12: Interpretation figure of the Springbok line. In the oceanic domain, oceanic layers 2A, 2B and 3 could be resolved between km 0 and km 50. Layer 2A changes gradually into a layer interpreted to contain synrift sediments and basaltic flows eastward of km 50. Here the transitional crust in underlain by a high-velocity, high-density body in the lower crust. These two domains are overlain by sedimentary successions that diminish towards the coast. From km 250 towards the east the crust is continental in origin and no sedimentary cover is observed.

Fig. 13: Model of the high-velocity bodies (v > 7km/s) interpreted for three seismic refraction lines recorded across the West African margin (for location see Fig. 1b) and the respective velocity distribution. The comparison shows the southward diminishing extent of this high-velocity bodies and the decrease in P-wave velocities from north to south.

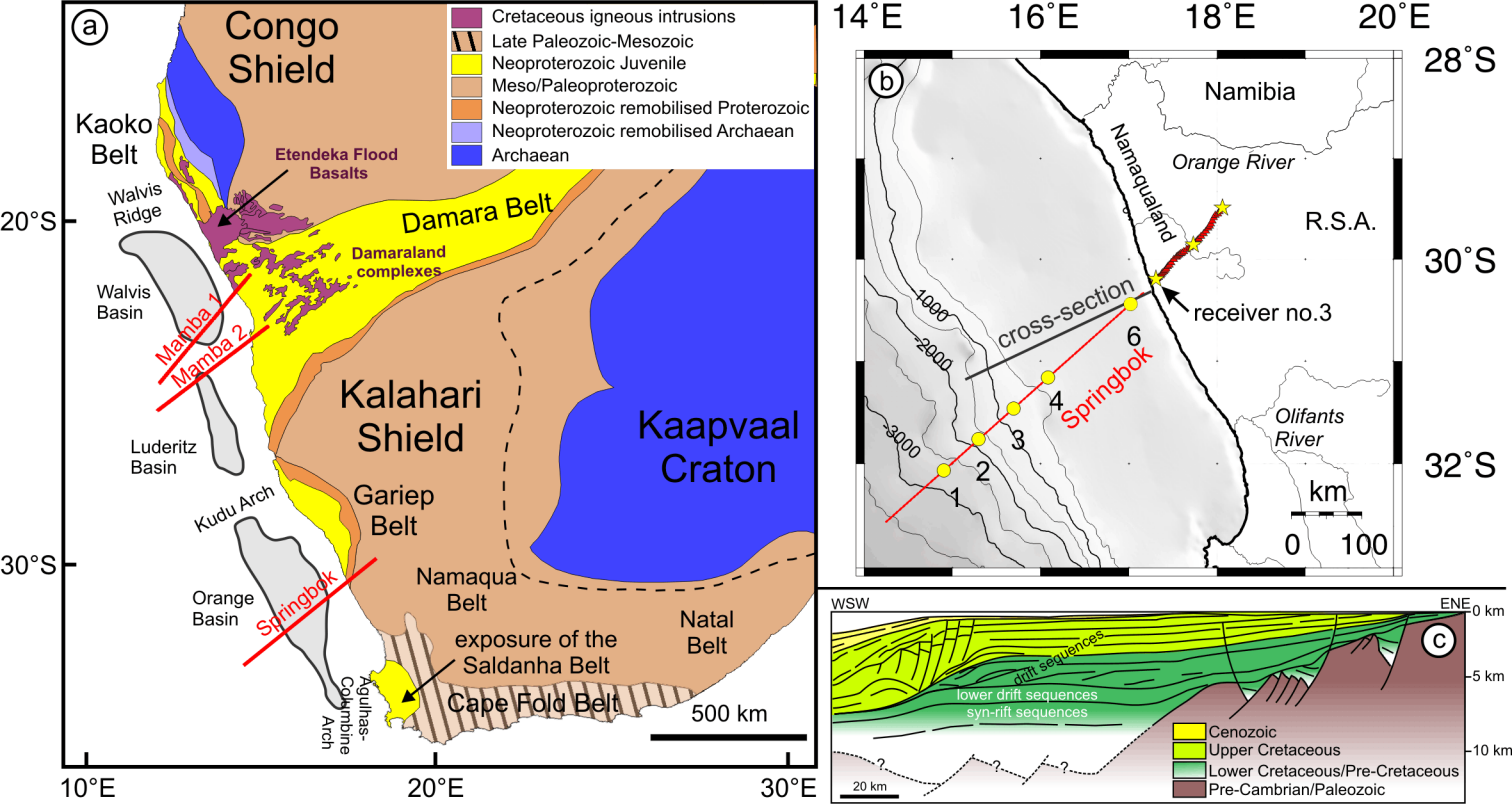
a
Congo Shield
Kaoko Belt
Etendeka Flood Basalts
Walvis Ridge
Damara Belt
Damaraland complexes
Walvis Basin
Mamba 1
Mamba 2
Kalahari Shield
Kaapvaal Craton
Luderitz Basin
Kudu Arch
Gariep Belt
Namaqua Belt
Orange Basin
Springbok
exposure of the Saldanha Belt
Natal Belt
Cape Fold Belt
Agulhas-Coloumbine Arch
500 km
Cretaceous igneous intrusions
Late Paleozoic-Mesozoic
Neoproterozoic Juvenile
Meso/Paleoproterozoic
Neoproterozoic remobilised Proterozoic
Neoproterozoic remobilised Archaean
Archaean
10°E
20°E
30°E
20°S
30°S
14°E
16°E
18°E
20°E
28°S
30°S
32°S
b
Namibia
Namaqualand
Orange River
R.S.A.
cross-section
receiver no.3
1000
2000
3000
1
2
3
4
6
Springbok
Olifants River
km
0
100
WSW
ENE
c
drift sequences
lower drift sequences
syn-rift sequences
Cenozoic
Upper Cretaceous
Lower Cretaceous/Pre-Cretaceous
Pre-Cambrian/Paleozoic
0 km
5 km
10 km
20 km

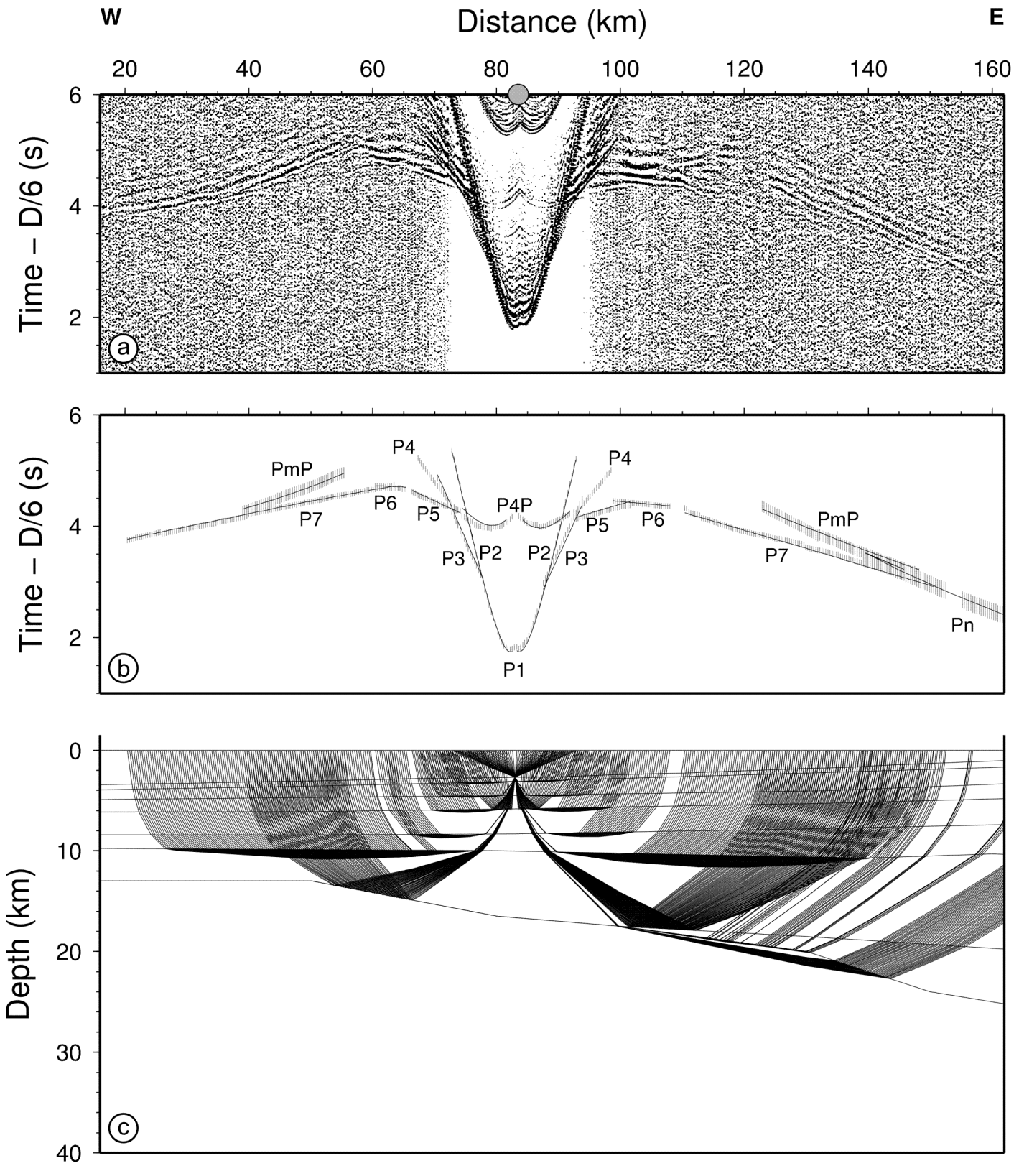
W
Distance (km)
E
20
40
60
80
100
120
140
160
Time – D/6 (s)
6
4
2
a
PmP
P7
P4
P6
P5
P4P
P3
P2
P2
P3
P5
P6
P4
PmP
P7
Pn
P1
b
Depth (km)
0
10
20
30
40
c

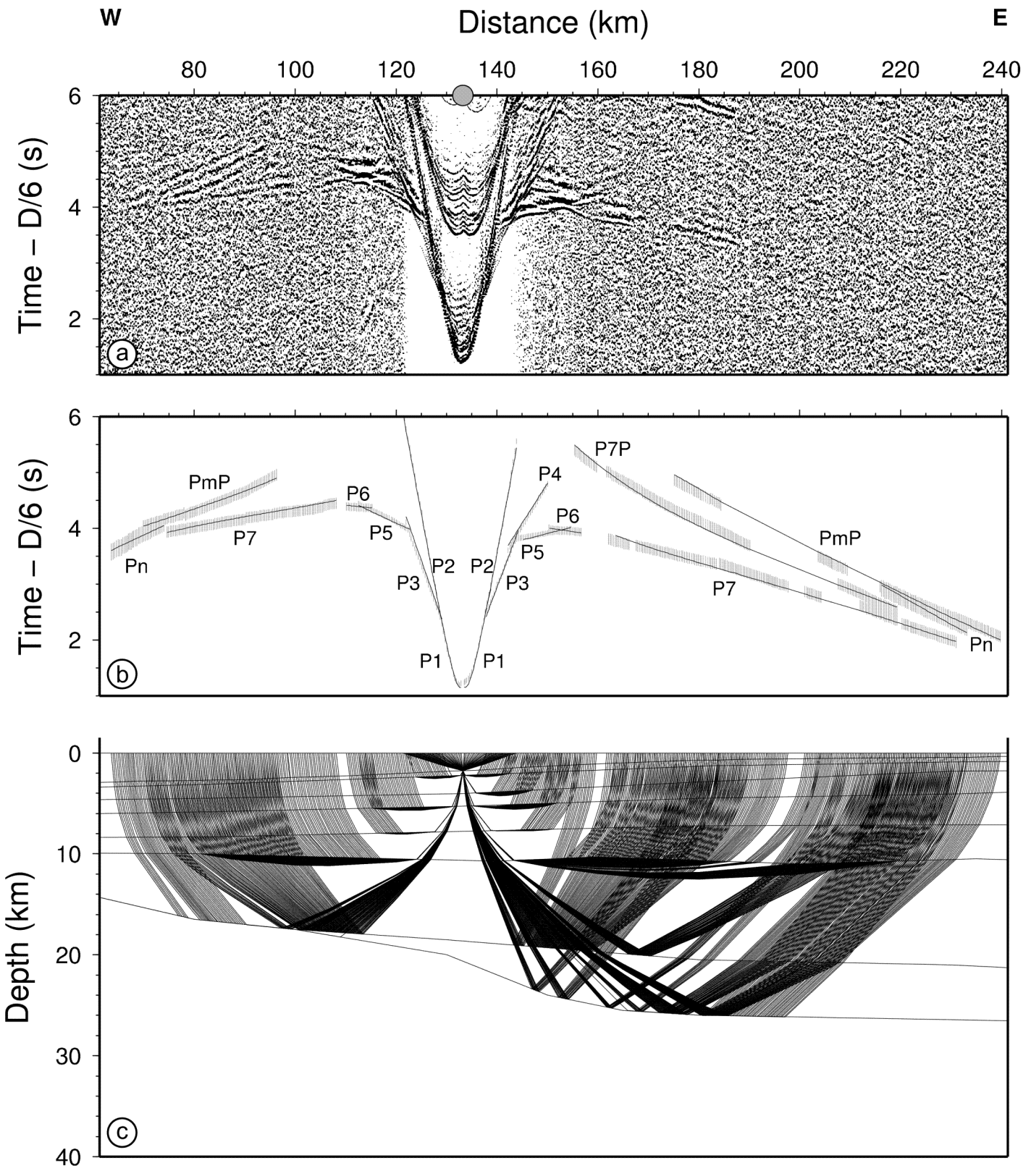
W
Distance (km)
E
80
100
120
140
160
180
200
220
240
Time – D/6 (s)
6
4
2
a
b
PmP
P7
Pn
P6
P5
P3
P2
P2
P3
P1
P1
P4
P6
P5
P7P
PmP
P7
Pn
Depth (km)
0
10
20
30
40
c

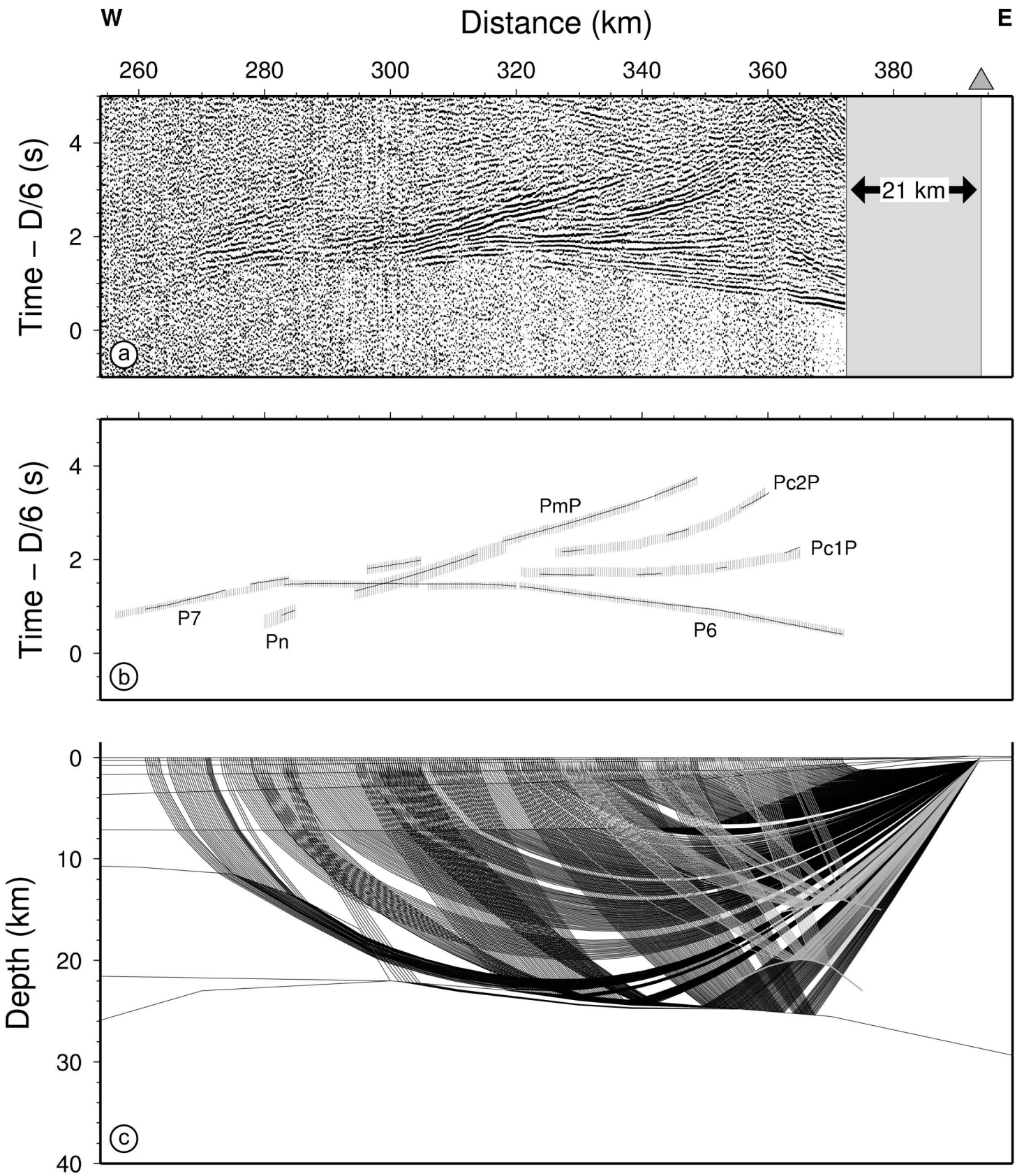
W
Distance (km)
E
260
280
300
320
340
360
380
Time – D/6 (s)
4
2
0
21 km
a
Time – D/6 (s)
4
2
0
PmP
Pc2P
Pc1P
P7
Pn
P6
b
Depth (km)
0
10
20
30
40
c

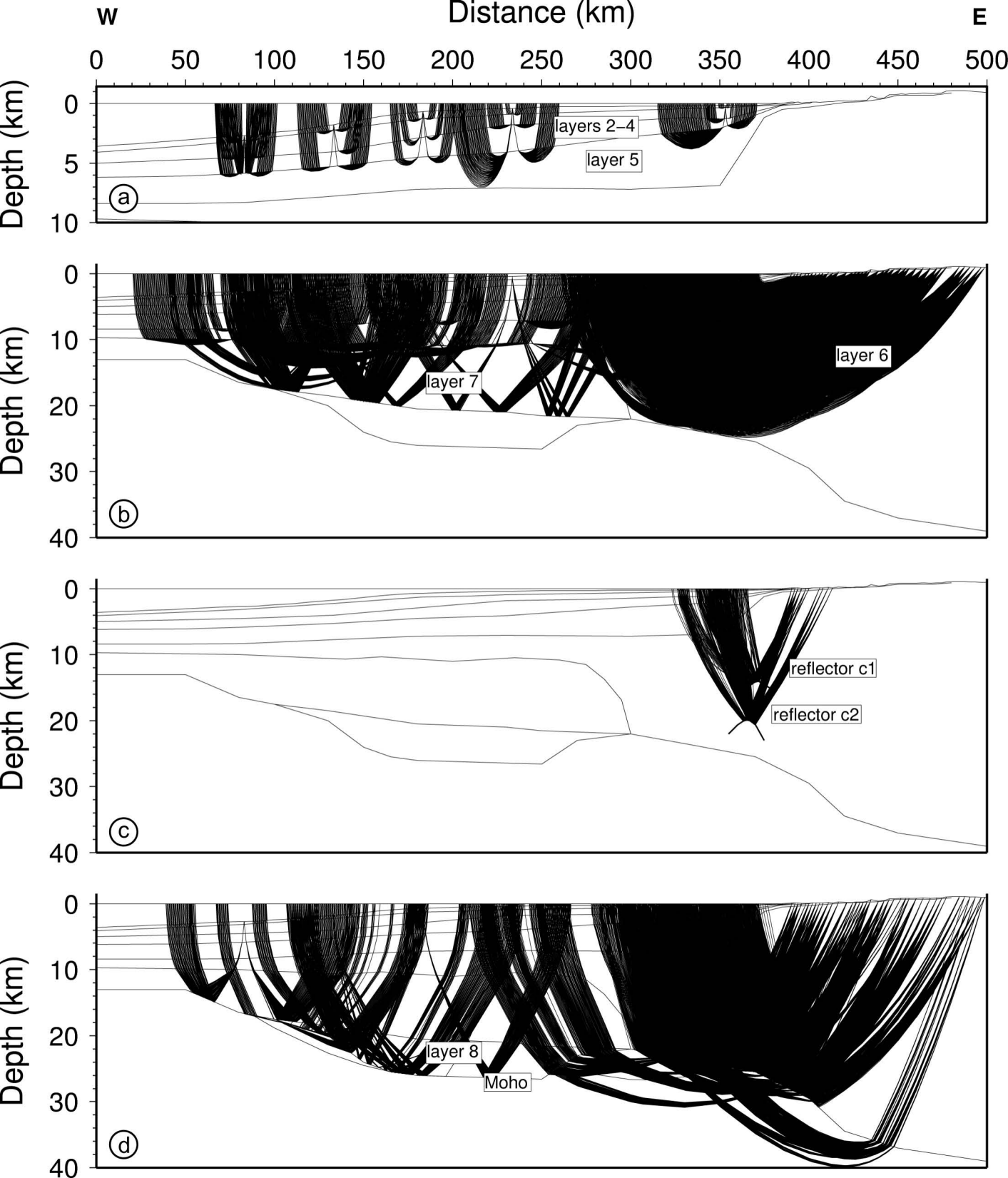
W
Distance (km)
E
0
50
100
150
200
250
300
350
400
450
500
Depth (km)
0
5
10
layers 2–4
layer 5
a
0
10
20
30
40
layer 6
layer 7
b
reflector c1
reflector c2
c
layer 8
Moho
d

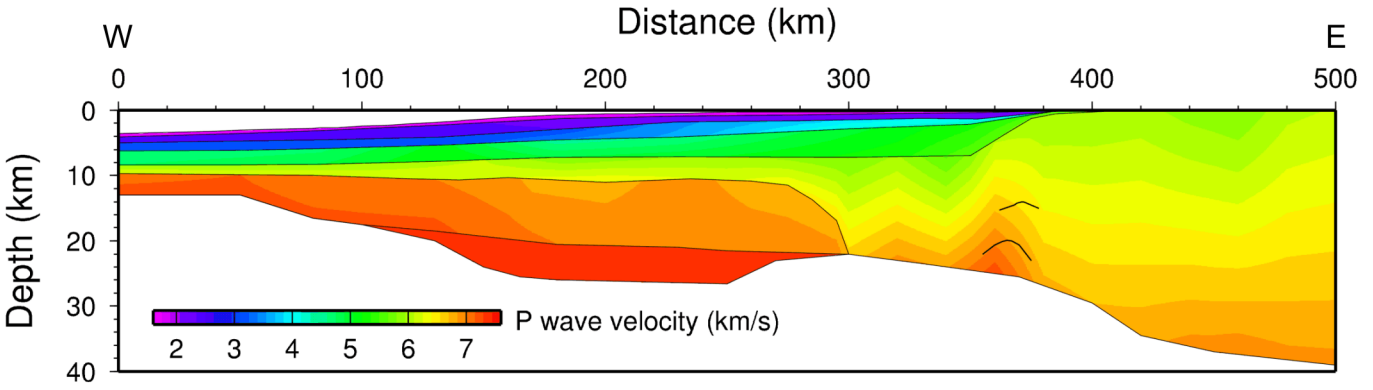
W
Distance (km)
E
0
100
200
300
400
500
Depth (km)
0
10
20
30
40
P wave velocity (km/s)
2
3
4
5
6
7

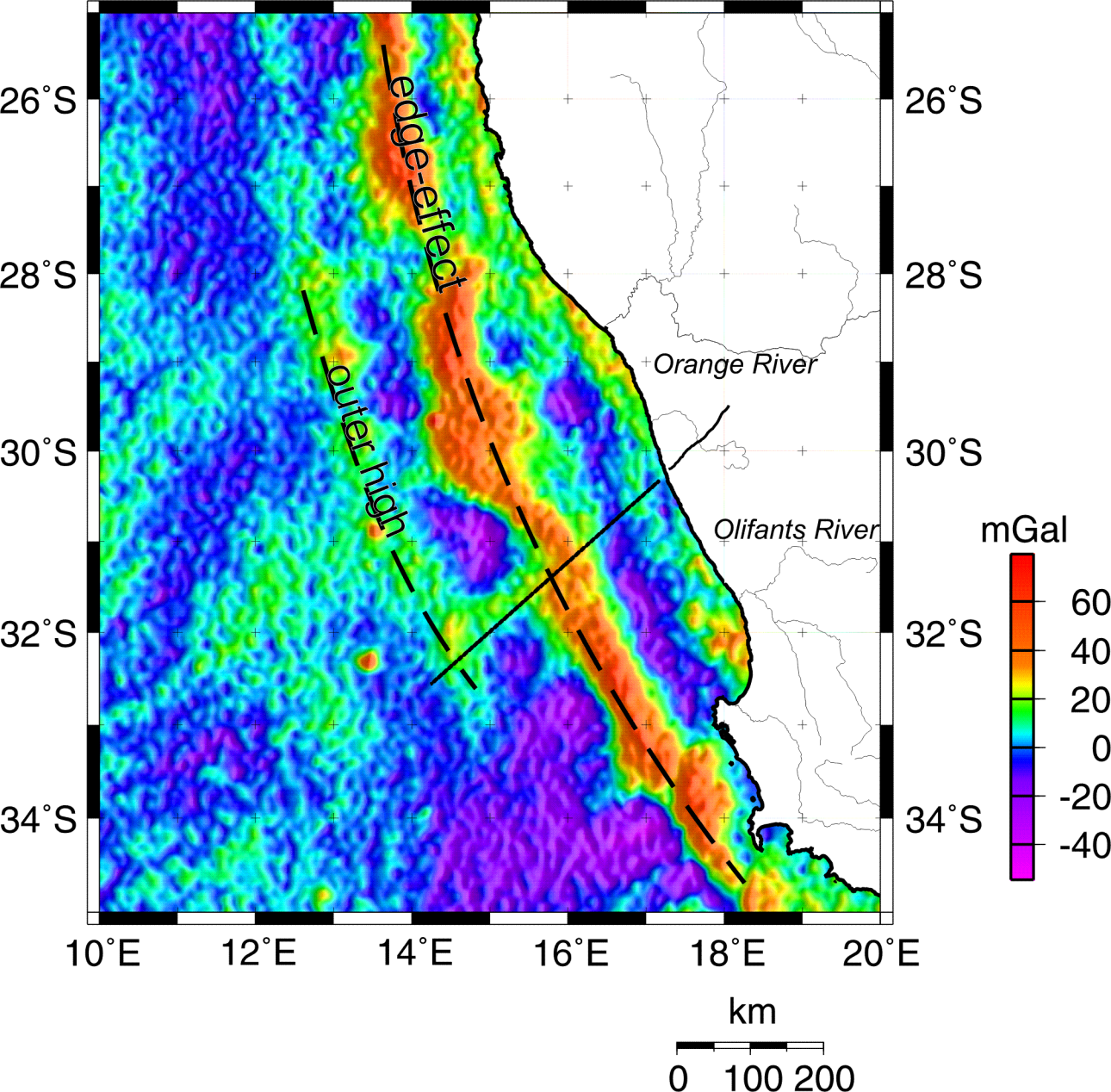
edge-effect
outer high
Orange River
Olifants River
mGal
60
40
20
0
-20
-40
26°S
28°S
30°S
32°S
34°S
10°E
12°E
14°E
16°E
18°E
20°E
km
0 100 200

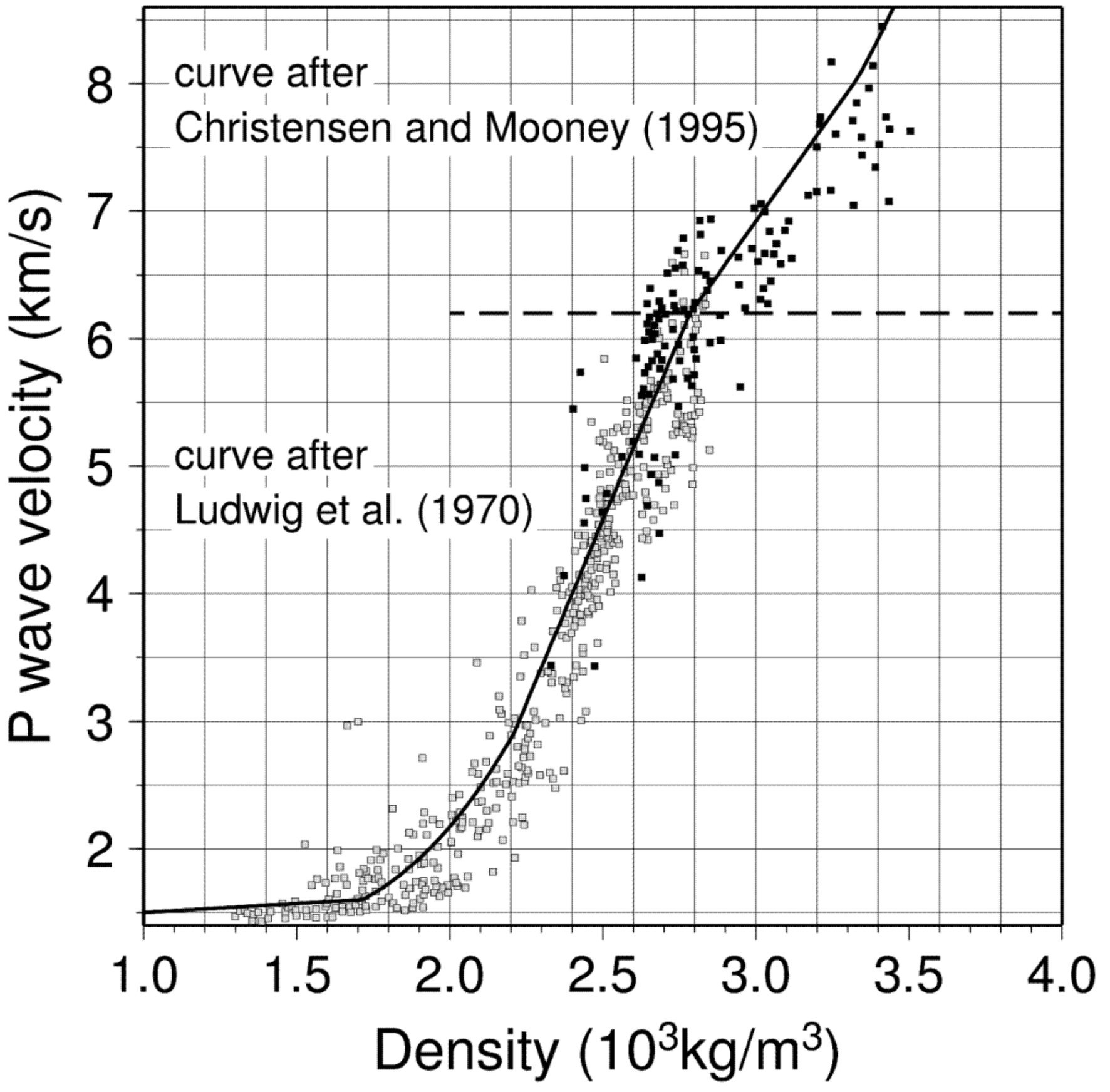
curve after
Christensen and Mooney (1995)
curve after
Ludwig et al. (1970)
P wave velocity (km/s)
Density (10³kg/m³)
2
3
4
5
6
7
8
1.0
1.5
2.0
2.5
3.0
3.5
4.0

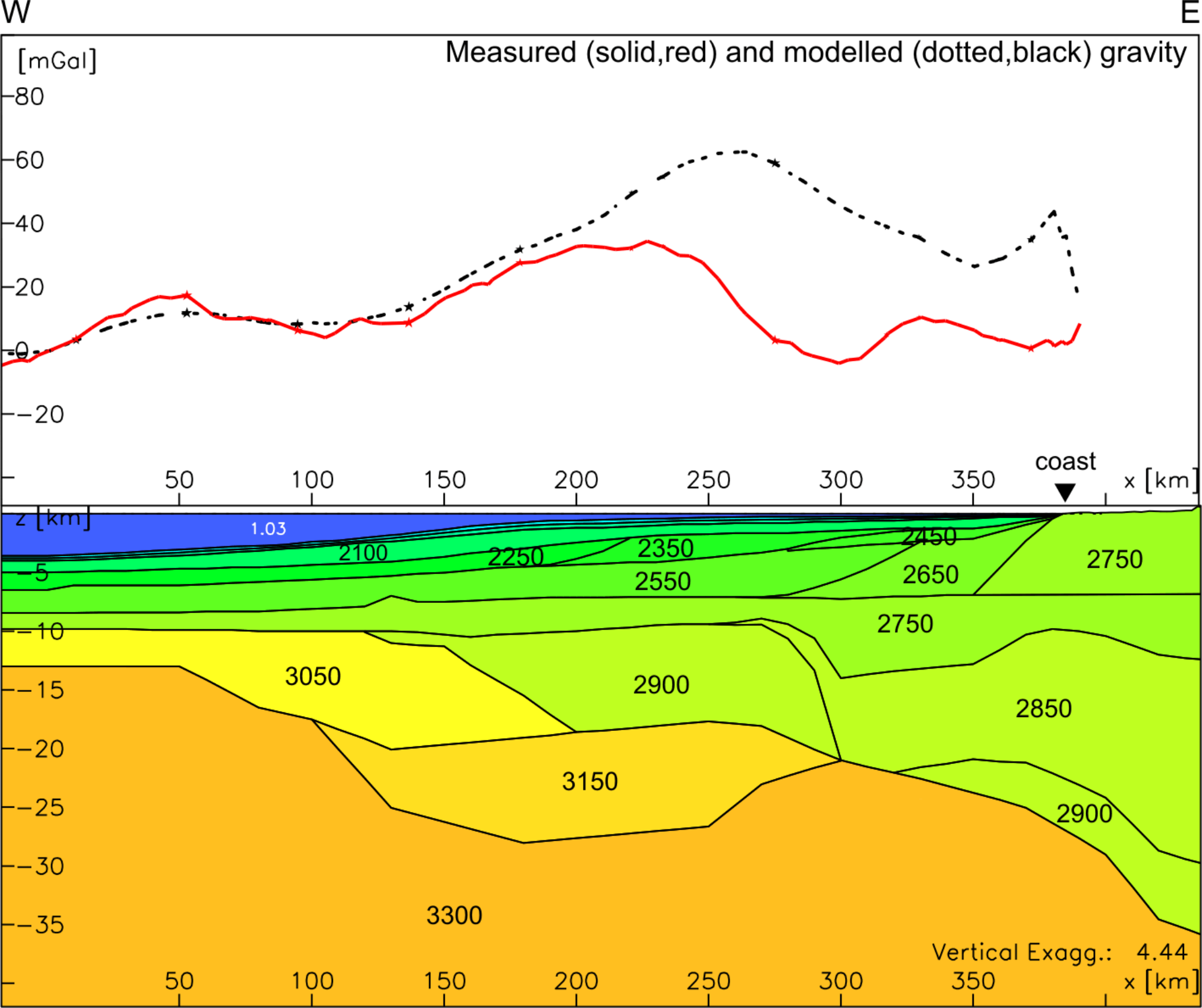
W
E
[mGal]
Measured (solid,red) and modelled (dotted,black) gravity
80
60
40
20
0
-20
50
100
150
200
250
300
350
coast
x [km]
z [km]
1.03
2100
2250
2350
2450
2550
2650
2750
2750
3050
2900
2850
3150
2900
3300
Vertical Exagg.: 4.44
5
10
15
20
25
30
35

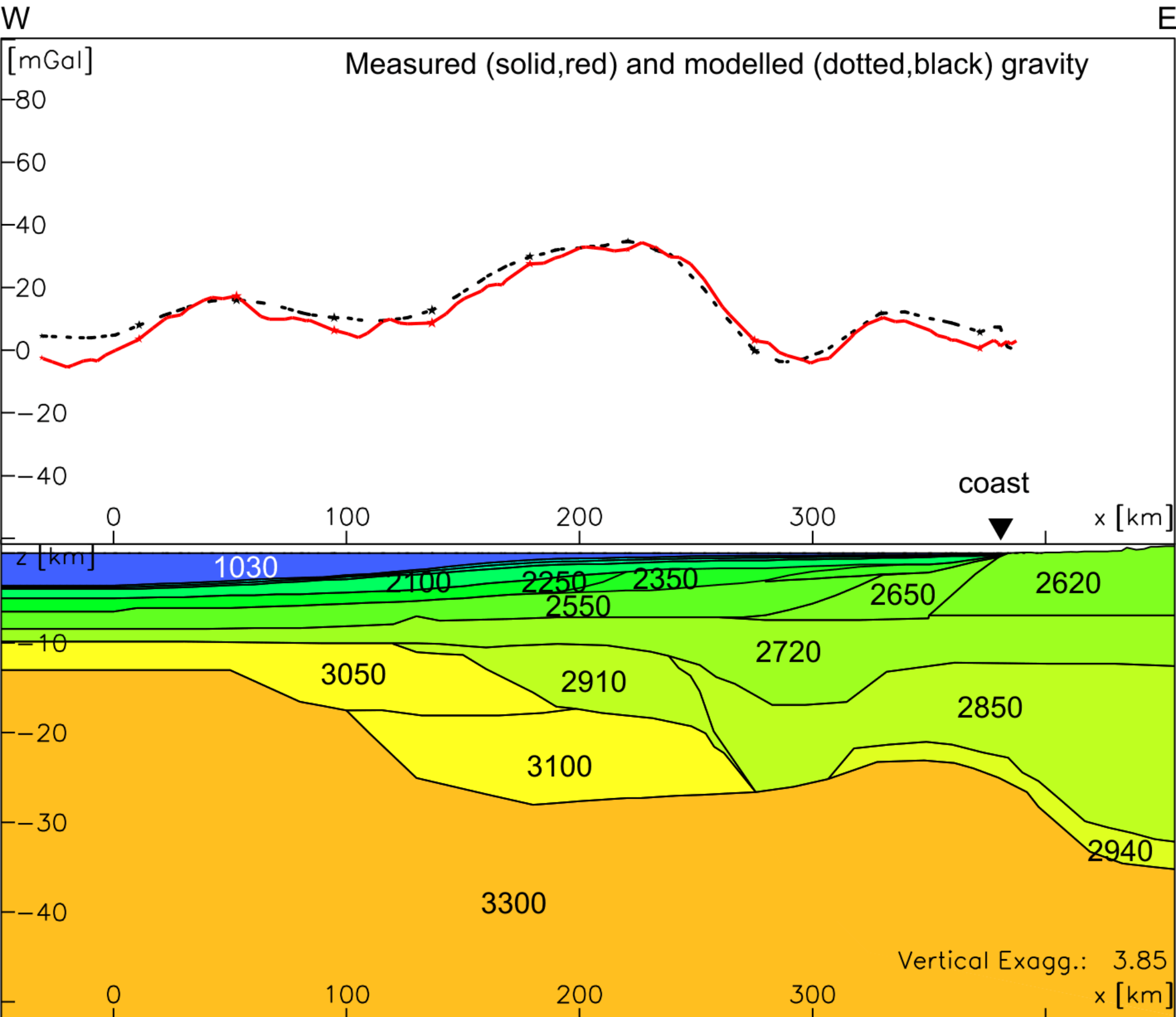
W
E
[mGal]
Measured (solid,red) and modelled (dotted,black) gravity
80
60
40
20
0
−20
−40
0
100
200
300
x [km]
coast
z [km]
1030
2100
2250
2350
2550
2650
2620
2720
−10
3050
2910
2850
3100
−20
−30
2940
3300
−40
Vertical Exagg.: 3.85
0
100
200
300
x [km]

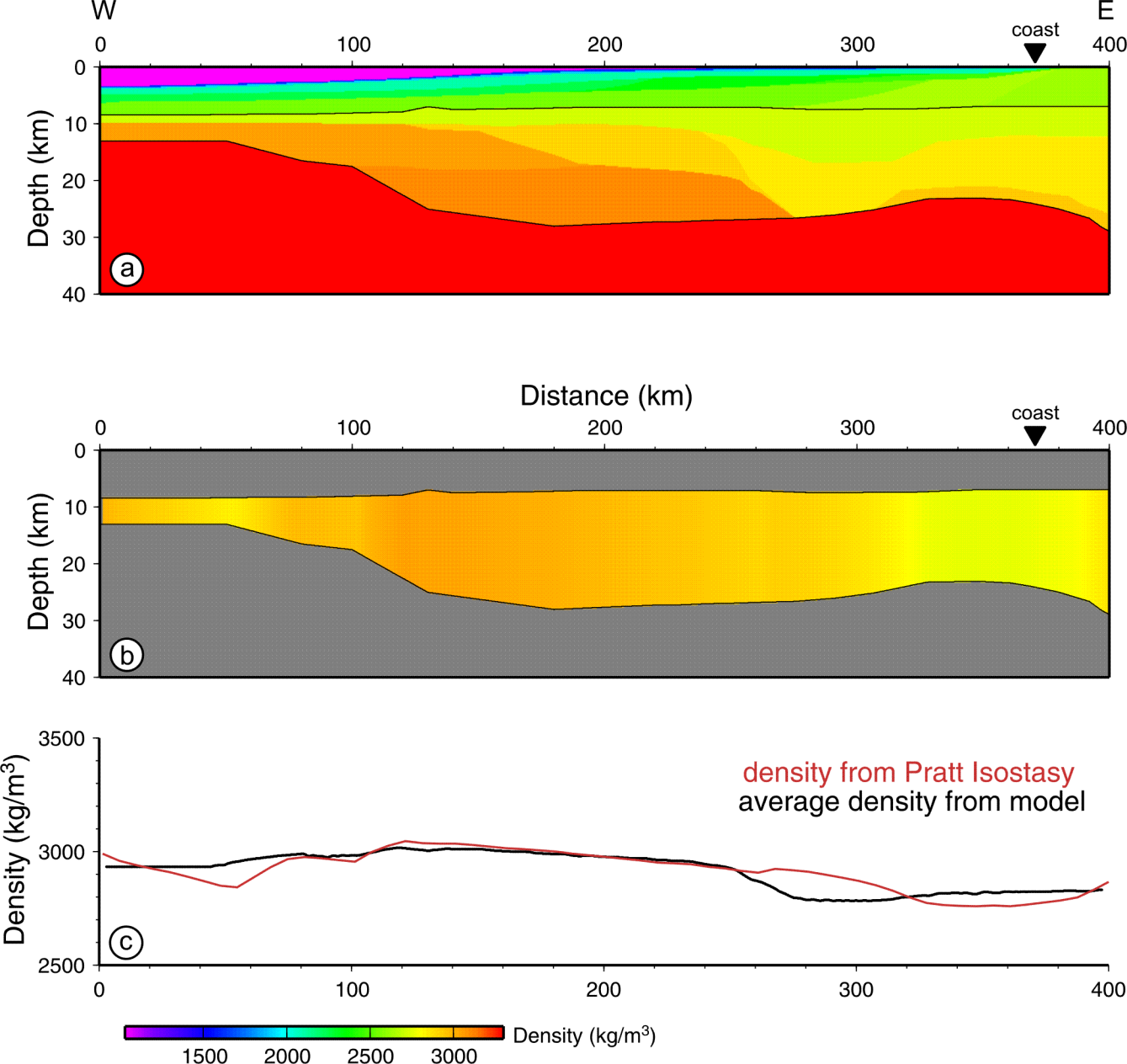
W
E
coast
0
100
200
300
400
Depth (km)
0
10
20
30
40
a
Distance (km)
b
3500
3000
2500
Density (kg/m3)
density from Pratt Isostasy
average density from model
c
1500
2000
2500
3000
Density (kg/m3)

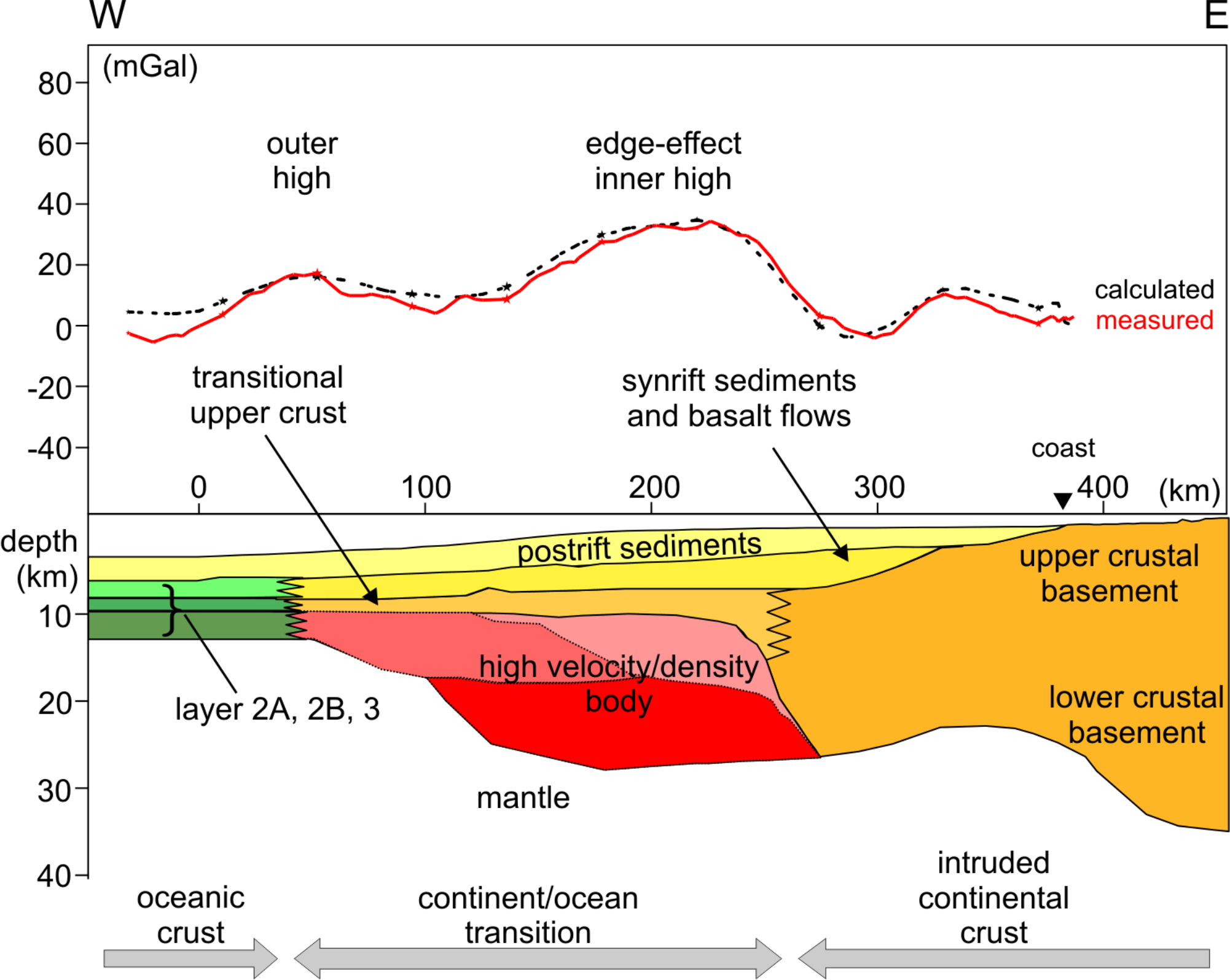
W
E
(mGal)
80
60
40
20
0
-20
-40
outer high
edge-effect inner high
calculated
measured
transitional upper crust
synrift sediments and basalt flows
coast
0
100
200
300
400
(km)
depth (km)
10
20
30
40
postrift sediments
upper crustal basement
high velocity/density body
lower crustal basement
layer 2A, 2B, 3
mantle
oceanic crust
continent/ocean transition
intruded continental crust

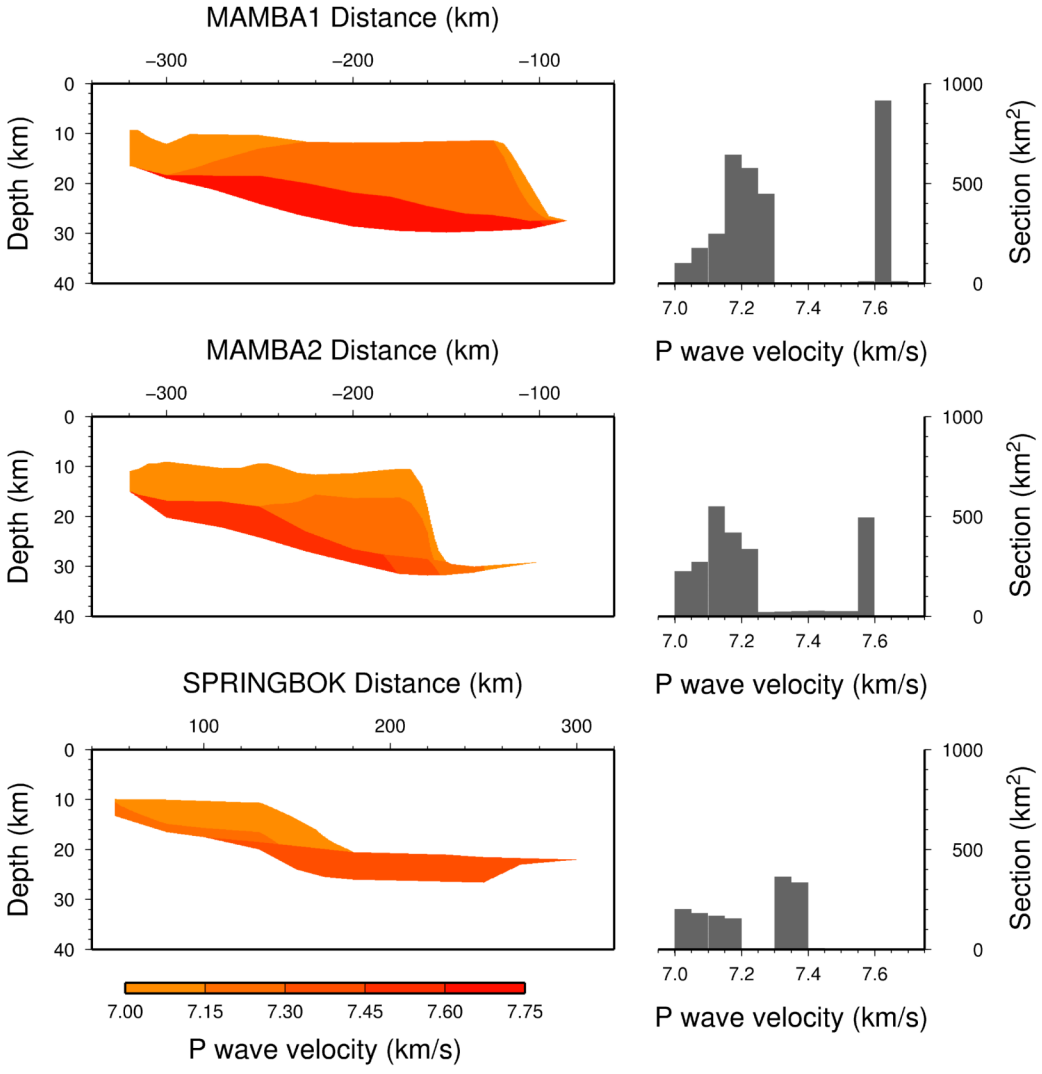
MAMBA1 Distance (km)
−300
−200
−100
Depth (km)
0
10
20
30
40
1000
500
0
Section (km²)
7.0
7.2
7.4
7.6
P wave velocity (km/s)
MAMBA2 Distance (km)
−300
−200
−100
Depth (km)
0
10
20
30
40
1000
500
0
Section (km²)
7.0
7.2
7.4
7.6
P wave velocity (km/s)
SPRINGBOK Distance (km)
100
200
300
Depth (km)
0
10
20
30
40
1000
500
0
Section (km²)
7.0
7.2
7.4
7.6
P wave velocity (km/s)
7.00
7.15
7.30
7.45
7.60
7.75
P wave velocity (km/s)